Structure, Interaction and Hydrogen Bond

Kun Dong, Qian Wang, Xingmei Lu, Qing Zhou, and Suojiang Zhang

Abstract Ionic liquids (ILs), as green solvents, have attracted amazing interest and their potential applications have prompted a large amount of research and investment, and some of the results have been inspiring. In recent years, in combination with cations and anions, some new ILs have been synthesized in the laboratory. However, compared with simple solid salts, the structures of ILs are complicated and their properties vary considerably. It is thus very time consuming to explore ILs experimentally when facing the huge number of ionic combinations. A molecular-based understanding can reveal the quantitative correlation between structures and properties, and is thus an important subject in the study of ILs. The unusual complexity of ionic interactions renders molecular-based interpretations difficult and gives rise to controversies about the structure of the ILs. Herein we discuss the ion-pair, cluster and X-ray crystals structures and their relationship with the properties of many typical ILs, especially imidazolium-based. In the ILs, apart from the strong electrostatic forces, non-covalent H-bonds and van der Waals (dispersion, induce forces) are examined and are shown to have a decisive effect on the properties of ILs.

Keywords Ionic liquid • Structure • Interaction • Property • Application

Beijing Key Laboratory of Ionic Liquids Clean Process, Key Laboratory of Green Process and Engineering, State Key Laboratory of Multiphase Complex System, Institute of Process Engineering, Chinese Academy of Sciences, Beijing 100190, PR China.

K. Dong • Q. Wang • X. Lu (✉) • Q. Zhou • S. Zhang (✉)
Institute of Process Engineering, Chinese Academy of Sciences, P.O. Box 353, Beijing 100190, China
e-mail: sjzhang@home.ipe.ac.cn; xmlu@home.ipe.ac.cn

S. Zhang et al. (eds.), *Structures and Interactions of Ionic Liquids*, Structure and Bonding 151, DOI 10.1007/978-3-642-38619-0_1,

1 Short Review of Ionic Liquids (ILs)

1.1 Synthesized ILs

Room temperature ionic liquids (RTILs) have been paid close attention by academia and the industries due to their environment-friendly properties, and particularly their potential in green chemistry. It is nearly 100 years since an IL, $[EtNH_3][NO_3]$, which has a melting point of 12°C, was first reported in 1914 [1]. Then research on RTILs renewed with the discovery of alkylpyridinium or 1,3-dialkylimidazolium haloaluminate salts by groups at the Air Force Academy in the mid-1970s. These salts were formed by mixing aluminum halides with the corresponding imidazolium or pyridinium halides [2]. Unfortunately, these haloaluminate ILs are highly sensitive to atmospheric moisture. In the 1990s, these salts with imidazolium-based cations incorporated with tetrafluoroborate or hexafluorophosphate anions were stable in the atmosphere and were regarded as a significant milestone in the development of ILs [3, 4]. By careful choice of the combination of these cations and anions it was possible to synthesize a large variety of ILs. Since 2000, more than 6,000 papers related to ILs have been published, with more than 1,000 in 2004, 1,300 in 2005, and nearly 1,900 in 2006 [5].

Non-haloaluminate RTILs share a common general structure of a bulky unsymmetrical "onium" organic cation associated with a weakly coordinating inorganic anion. So far, the most popular cations are 1,3-dialkylimidazolium-, *N*,*N*-dialkylpyrrolidinium-, *N*,*N*,*N*,*N*-tetraalkylammonium-, and *N*-alkylpyridinium-based. Concerning their anionic counterparts, tetrafluoroborate ($[BF_4]^-$), hexafluorophosphate ($[PF_6]^-$), bis(trifluoromethylsulfonyl)amide ($[NTf_2]^-$), and triflate ($[OTf]^-$) are the most common. Figure 1 shows some cations and anions commonly used for the preparation of RTILs [6, 7].

RTILs have been attracting interest because of the many unique properties they are supposed to have. RTILs have negligible vapor pressure and are thus nonflammable and nonvolatile, largely decreasing the chance for fugitive emissions. They show high thermal stability, with decomposition temperatures around 300–500°C. They are able to solvate a large variety of organic and inorganic compounds, either polar or nonpolar. They are generally regarded as polar yet noncoordinating solvents. They display a good intrinsic conductivity and are extremely redox-robust. Actually, as a result of the intense research dealing with their physicochemical properties, it has become clear that the above-mentioned properties cannot be considered as generic properties for these media. For instance, it has been shown that many ILs decompose above 80–90°C.

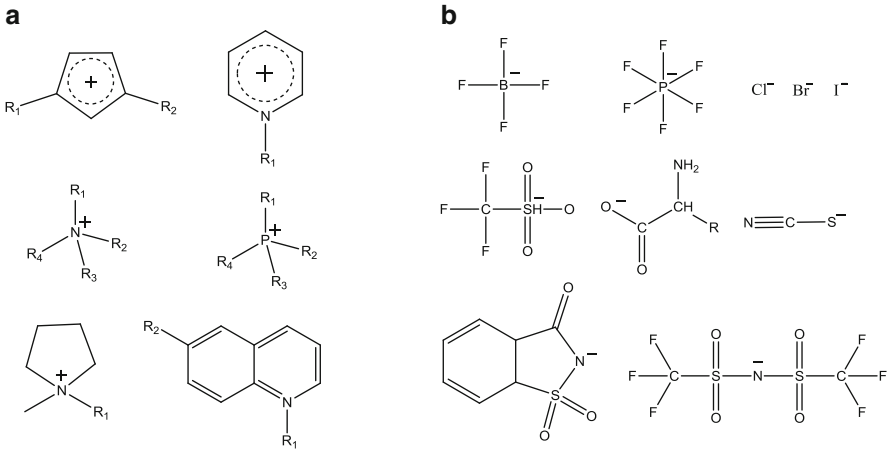

Fig. 1 Cations and anions studied: (**a**) cations; (**b**) anions

1.2 Relationship between Properties and Structures of ILs

Melting Points (T_m). Many properties of ILs are special and show prospects for applications. ILs are completely composed of ions, but the unusually low melting points exceed expectations. Melting points of many ILs are lower than 0°C; even the melting point of [Emim][$N(SO_2CF_3)_2$] is −16°C [8]. The low melting points are related to the structures and molecular packing of ions. An increase in size, anisotropy, and internal flexibility of the ions should lower the melting point, as shown in Table 1. The symmetry and length of alkyl chain of cations also influence the melting point, and the short *N*-alkyl chains and higher molecular symmetry can frequently increase the melting point. The melting point of [Mmim]Cl IL is 124.5°C and of [Bmim]Cl is 65°C. A simple rule is that cations with short *N*-alkyl chains ($C_n \leq 3$) form crystalline phases with high melting points, and ILs with 4 ~ 10 *N*-alkyl chains exhibit a broad liquid range with low melting points and a remarkable tendency to supercool. When the *n* in C_n is larger than 10, the salts show a complex phase behavior [10].

Viscosity (η). RTILs are viscous liquids, their viscosities being one to three orders of magnitude higher than those of conventional solvents [11]; obviously that is not very helpful for some applications and it may exert a strong effect on the rate of mass transport within solution and on the conductivity of the salts. The viscosity of the RTILs strongly depends on the nature of the anion [12–14]. ILs containing $[NTF_2]^-$ anion present the lower viscosity, for instance, the viscosity of [Emim][NTf_2] IL is 25 mPa·S as shown in Table 1, but viscosity is higher for RTILs containing $[PF_6]^-$ nonplanar symmetric anions, and the viscosity of [Bmim][PF_6] IL is 308 mPa·S [15]. It has been suggested that the size, shape, and molar mass of the anion contribute to the viscosity with smaller, lighter, and more symmetric anions leading to more viscous RTILs [16]. Additionally, the relative basicity of the

Table 1 Properties of the typical 1-ethyl-3-methylimidazolium-based ILs

Anion	Melting point (°C)	Viscosity (mPa·S)	Conductivity ($S \cdot m^{-1}$)	Enthalpy of Vap. (298.15 K, $kJ \cdot mol^{-1}$)
Cl^-	87			196.1 (363.15 K) [9]
$[BF_4]^-$	11	37–66.5	1.58–1.38	182.2
$[PF_6]^-$	62		0.52	189.0
$[TfO]^-$	−9	45	0.86	
$[NTf_2]^-$	−16	25–34	0.91	135.0

anions and their ability to form H-bonds or to allow van der Waals attractions also have a pronounced effect on viscosity. The fluorinated anions such as $[BF_4]^-$, $[PF_6]^-$, or $[BETI]^-$ form ILs with higher viscosity due to the formation of H-bonds or stronger van der Waals forces, but salts with $[N(CN)_2]^-$ and $[C(CN)_3]^-$ anions exhibit low viscosity. Compared to anions, cations have secondary effects on the viscosities of ILs. For any of the cation types, increasing the length of alkyl chains results in higher viscosities because of stronger van der Waals interactions between larger cations [17, 18].

Temperature has a remarkable effect on the viscosity of ILs. Okoturo et al. found that the viscosity decreases when the temperature increases. The correlation can be described by the Vogel-Tammann-Fulchers equation:

$$\ln \eta = \ln \eta_\infty + \frac{E_\eta}{RT} \tag{1}$$

where η_∞ is the viscosity of infinite high temperature E_η is the energetic barrier of ionic motion.

Conductivity (Λ). Conductivity is a property of primary importance and most electrochemical processes are related to the conductivity of the ILs. Being composed of ions, ILs are supposed to be among the most concentrated electrolytes with many charge carriers per unit volume. Some ILs exhibit higher conductivity, and the order of 10 $mS \cdot cm^{-1}$ can be found in the imidazolium family (Table 1). However, quaternary ammonium ILs exhibit lower conductivity, and the highest conductivity is 2 $mS \cdot cm^{-1}$, found in *N*, *N*-dialkylpyrrolidinium bis(trifluoromethylsulfonyl)amide.

As mentioned previously, the high viscosity of RTILs has a major impact on the conductivity because the conductivity is inversely linked to the viscosity [16, 18, 19]. The less viscous $[NTf_2]^-$ salts usually exhibit among the highest conductivities [20]. However, quantitative correlations have not been observed between viscosity and conductivity in most ILs. For instance, [Emim][TfO] and [BMIm][NTf_2] display similar viscosities and densities, but the conductivity of [Emim][TfO] is 0.29 $mS \cdot cm^{-1}$ and [Bmim][NTf_2] is 0.91 $mS \cdot cm^{-1}$, and their conductivities differ by a factor of 2. Many others factors also influence the conductivity, such as ion size and aggregation, anionic charge delocalization, and correlated ionic motions

[13, 16, 21]. The Nernst-Einstein equation relates the molar conductivity to the self-diffusion coefficients of ions. However, the values predicted by

$$\Lambda = \frac{F^2}{RT}(D_{cation} + D_{anion}) \tag{2}$$

are not in good agreement with experimental measurements, and experimental values are smaller than the theoretical values, which can be rationalized by a coupled and clustered aggregation motion of cations and anions in electrically neutral configuration, but the neutral species cannot contribute to the ionic conductivity. On the other hand, increasing the length of the *N*-alkyl chains of cation results in a higher viscosity and a lower conductivity.

Enthalpy of Vaporization (ΔH). An important property of ILs is nonvolatility such that the ILs are green and able to substitute for environmentally contaminating volatile organic chemicals (VOCs). However, Earle et al. [22] found that many RTILs can be distilled and not decomposed at higher temperature and lower pressure. Owing to the strong ionic interactions, the molar enthalpies of vaporization of the ILs are by almost an order of magnitude higher than for typical molecular liquids, as shown in Table 1. The anionic symmetry has the obvious effect on the vaporization of IL, and the ILs with more symmetric anions, Cl^-, $[BF_4]^-$, and $[PF_6]^-$, have higher enthalpy of vaporization than $[NTf_2]^-$ salt. However, these ILs can decompose in the gas phase, for example, [Emim]Cl thermally decomposes when heated to 190°C in vacuum. The volatile decomposition products are 1-methylimidazole, 1-ethylimidazole, chloromethane, chloroethane, ethane, and hydrogen chloride species, but the $[NTf_2]^-$ anionic salts are thermally stable and may be heated to 600 K. Thus most vapor measurements have been carried out on ILs by different methods (isothermogravimetry, Knudsen-type effusion, surface tension, etc.). In such studies it was found that increasing the length of alkyl chains of cation leads to a larger enthalpy of vaporization, the enthalpy values being 135, 155, 173, and 192 $kJ \cdot mol^{-1}$ for $[C_2mim][NTf_2]$, $[C_4mim][NTf_2]$, $[C_6mim][NTf_2]$, and $[C_8mim][NTf_2]$, which indicates the long alkyl chain leads to stronger interactions between cations and anions [23, 24].

1.3 Hydrophilic and Hydrophobic

The presence of water in ILs can greatly influence the quality of ILs, including viscosity, polarity, and conductivity, and can also influence the solubility of other substance in RTILs. For example, the presence of water in $[Bmim][PF_6]$ IL has resulted in the underestimation of the solubility of CO_2 in the ionic liquid [25]. These imidazolium-based ILs present different hydrophilicities. Anions such as halide, pseudo-halide, $[BF_4]^-$, methyl sulfate, $[NO_3]^-$, and $[ClO_4]^-$ are

hydrophilic, which significantly limits their usages, while ionic liquids with anions such as $[PF_6]^-$, $[SbF_6]^-$, $[OSO_2CF_3]^-$, $[OCOCF_3]^-$, etc. are hydrophobic and have potential in some industrial applications. However, it is also clear that the commonly called "hydrophobic" ILs are actually hygroscopic and can absorb a certain amount of water from the air [17].

T. Welton et al. have investigated the state of water in many imidazolium-based ILs by ATR and transmission IR spectroscopy [26]. They found that anions are mainly responsible for the solubility of water. In these ILs, the water is not associated together but bound by H-bonds with anions with concentrations of dissolved water in the range 0.2 ± 0.1 mol $\cdot$ dm^{-1}. The water molecules at these concentrations exist in symmetric 1:2 type H-bonded complexes: anion. . .H–O–H. . .anion. Additional evidence can be seen from Table 2 that the shifts of antisymmetric ν_3 and symmetric ν_1 bands of water molecules in the listed ILs roughly follow the relationship of $\Delta\nu_3 = 1.17\Delta\nu_1 - 0.60$. The strength of H-bonds between the H_2O molecule and anions can be estimated from the wave number shift ($\Delta\nu$) between ν_3 of water in vapor phase and that dissolved in ionic liquids by Eq. 3 [27]:

$$\Delta H = -80({\nu_3}^{vapor} - {\nu_3}^{IL})/{\nu_3}^{vapor} \tag{3}$$

(where ΔH is the enthalpy of H-bond, KJ/mol). It can be seen that the different anion can interact with water by the different strength of H-bonds as listed in Table 2. In addition, the water contents absorbed from the open air have a consistent trend with the strength of the H-bonds; for example, the contents of water in [Bmim][PF_6], [Bmim][BF_4], and [Bmim][$(CF_3SO_3)_2N$] increase by the order of 2,640, 19,500, and 33,090 ppm by Karl-Fischer at relative humidity 59 % [26]. It implies that the H-bond play an important role for the solubility of water in ILs.

Although the cation plays a secondary role for the solubility of water in bulk ILs, at the vapor-liquid surface the water mainly interacts with the imidazolium cations. The hydrophobic ILs display a dramatic reorientation at the gas-liquid interface as water contacts the surface. It had been shown by sum frequency generation (SFG) of the C–H stretching mode that C–H groups, especially the C_2–H group in ring contact with water by C–H. . .O H-bond interaction, produces a tilting of the cation on the surface. Where the plane of the ring will be, either parallel or perpendicular to the alkyl chain, is dependent on the protonation or methylation of the C_2 position [28, 29].

Generally speaking, the properties presented are important for the application of ILs, especially basic scientific data; however some data are difficult to measure directly. However, the properties of ILs strongly depend on the structures and anion–cation combination styles, and understanding of the structures and the ionic interaction will provide a more convenient way to estimate thermodynamic data prior to practical process design.

Table 2 The shifts of the $\nu 3$ and $\nu 1$ (cm^{-1}) of water in different ionic liquids (with $[Bmim]^+$ cation) compared with the corresponding water bands in vapor and the enthalpies of H-bonding [26]

Anion	$\Delta\nu 3$	$\Delta\nu 1$	$-\Delta H$ ($kJ \cdot mol^{-1}$)
$[PF_6]^-$	84	62	7.5
$[SbF_6]^-$	93	77	8.3
$[BF_4]^-$	116	97	9.6
$[(CF_3SO_2)_2N]^-$	119	97	10.5
$[ClO_4]^-$	143	117	12.5
$[(CF_3SO_2)_2N]^-$	151	113	13.4
$[CF_3SO_3]^-$	181	151	15.9
$[NO_3]^-$	236	207	20.1

2 Structures of ILs

In recent years, some new ILs were synthesized in the laboratory, and the number of possible cation and anion combinations has increased significantly such that researchers believe the one trillion RTIL could possibly be prepared [30]. The synthetic problem of being able to design RTILs rationally through variation of the anion and cation still remains to be thoroughly investigated, despite attempts to correlate structures with properties. It is thus essential to develop a systematic method of selectively choosing a given ion pair to be used as a predictive tool in the rational design of new ILs.

A structurally based understanding is a great challenge because the molecular and electronic structure, charge distribution, and orbital overlap of ions, give rise to complex interactions and forces involved in the electrostatic, hydrogen bonds, and van de Waals interactions. Currently there has been substantial growth in the number of theoretical investigations pertaining to ILs, whereby scientists are attempting to predict many of the physical properties and have produced results agreeing with experimental values. Many quantitative correlations have also been established to help predict physic-chemical properties and accelerate the exploration for new ILs [31].

2.1 Dialkylimidazolium-Based Halides ILs

Unlike ionic solid materials, for example NaCl, in which the molecules and ions can be packed close to each other, leading to high lattice energy, the halide anionic ILs are liquid state at ambient temperature, although the strong electrostatic interaction – the bulkiness of both the cation and anion – prevents such packing, thereby lowering the lattice energy.

Halide anionic ILs have already been studied and the anions were found mainly to involve chloride, bromide, and iodide. However, a fatal defect of the class of ILs is their moisture problems in the atmosphere; thus their applications are very limited. In recent years, ILs (1-ethyl-3-methylimidazolium halides ([Emim]X, X = C1 or Br)) have been mixed with the corresponding aluminum(III) halide (AlX_3, X = C1 or Br) to produce the halogenoaluminate ILs, in which the anions

Table 3 Crystallographic data of 1-ethyl-3-methylimidazoium halides ILs [32, 33]

ILs	[Emim]Cl	[Emim]Br	[Emim]I
Chemical formula	$C_6H_{11}ClN_2$	$C_6H_{11}BrN_2$	$C_6H_{11}IN_2$
M	146.62	191.1	238.07
Space group	$P2_12_12_1$	$P2_1/c$	$P2_1/c$
Crystal system	Orthorhombic	Monoclinic	Monoclinic
a/nm	1.0087	0.8749	0.8789
b/nm	1.1179	0.7999	0.8130
c/nm	2.8733	1.2662	1.3364
V/nm^3	3.240	0.8332	0.9117
D/g · cm^{-3}	1.204	1.520	1.730

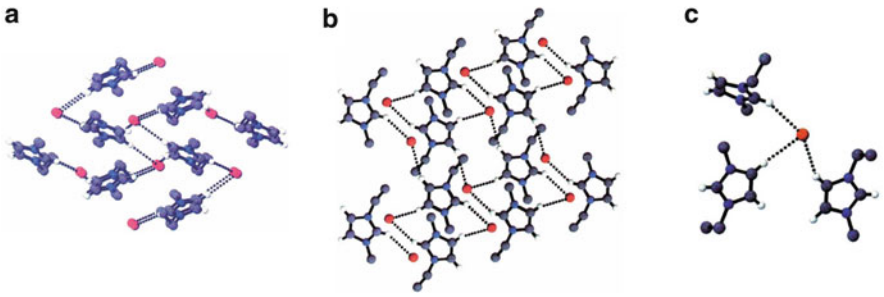

Fig. 2 The packing of ions in solid [Emim]Br (**a**) and [Emim]I (**b**), and the local ionic structure (**c**) [32]. The *dashed lines* showed the H-bonded interactions

exist as $[AlX_4]^-$ and $[Al_2X_7]^-$. Halogenoaluminate(III)-based ionic liquids, which may be used to investigate a wide range of industrially important chemistry, have been of particular interest [32].

The ILs are solid at ambient temperature and their crystallographic data are collected in Table 3. The [Emim]Cl IL is an orthorhombic crystal system, but similar solid structures were found in [Emim]Br and [Emim]I. Starting with the coordinates from the iodide structure, refinement by full-matrix least squares, with non-hydrogen anisotropic atoms and hydrogen isotropic atoms, was used to solve the structure.

Figure 2 shows the packing of ions and local structures in the crystals of [Emim]Br and [Emim]I. The structures consist of different layers of anions and cations which are interconnected by the extensive H-bonds (Fig. 2a, b). Each cation is hydrogen bonded to three anions and each anion is hydrogen bonded to three cations (Fig. 2c). The local structure around the cation is superficially similar to that observed for [Emim]Cl, but the overall morphology of the crystals is somewhat different.

Figure 3 shows the pairwise molecular structures of 1-ethyl-3-methylimidazolium and 1-butyl-3-methylimidazolium halides salts from ab initio calculations with the lowest interactive energies [34]. [Emim]Cl has four different ionic structures (Fig. 3), and the chloride ion with coplanar structures is more stable. Chloride ion, found in the plane of the ring, is associated with the hydrogen of C2 of

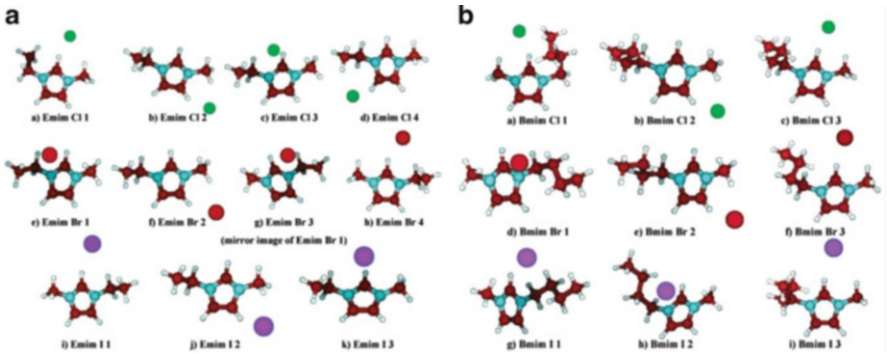

Fig. 3 1-Ethyl-3-methylimidazolium (**a**) and 1-butyl-3-methylimidazolium (**b**) halide ion pair structures with lowest interactive energies by ab initio calculations [34]

the ring, positioned closer to the methyl substituent as opposed to the ethyl substituent, which is agreeable with crystal structure. [Emim]Br has three different ionic structures (Fig. 3). The first (Emim Br 1 in Fig. 3) was found to be the most stable structure, and the third (Emim Br 3 in Fig. 3) coalesced with the first at the MP2 levels. Unlike the chloride system, where the chloride was found to be coplanar with the ring, the bromide of the most stable structure was found to be above the ring plane, which was a significant difference with respect to the position of the bromide in the crystal structure and the crystal structure indicates that the bromide resides in the ring plane (Fig. 3). The [Emim]I have two different structures, wherein the anion is within the plane of the ring. The first is the most stable structure (Emim I 1 in Fig. 3), agreeing with the crystal structure. The H-bond distance in the calculated structure (0.285 nm) was found to agree with the literature (0.293 nm).

Gross trends relating interaction energies and melting points were found within the chloride, bromide, and iodide series (see Fig. 4). From the figure it can be seen that the iodide series with the different chain lengths exhibit a "linear" trend, in which the melting points were found to decrease with increasing chain length, and this was associated with a decrease in the magnitude of interaction energy. In the cases of the chloride and bromide anions, the melting points of the $[Pmim]^+$ analogue were significantly lower than those of the $[Emim]^+$ and $[Bmim]^+$ analogues, although the interaction was found to increase in magnitude with increasing alkyl chain length. For the bromides, the structures were different, which introduces some scatter in the results. A trend was also found to exist in the $[Bmim]^+$ halide series, where the melting point increase between [Bmim]Cl and [Bmim]Br was associated with an increase in magnitude of the interaction. The melting point was then found to decrease significantly between [Bmim]Br and [Bmim]I, and this was associated with a significant decrease in magnitude of the interaction.

The preliminary investigation of a series of three imidazolium-based cations paired with three halide anions provides some initial hints as to the relationship

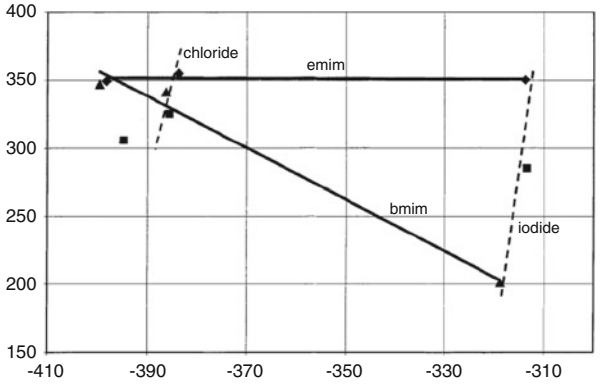

Fig. 4 Correlation between melting points and the binding energies for halide-based ionic liquids: $[Emim]^+$ (*filled diamonds*); $[Pmim]^+$ (*filled squares*); $[Bmim]^+$ (*filled triangles*) [34]

between the interaction energies and the melting points. The result suggests that there is more than one factor contributing to the melting point behavior of ILs. It is possible that for certain systems the melting point is governed more strongly by the cation than the anion and vice versa, with a balance between Coulombic attractions of oppositely charged ions and Van der Waals repulsions of the alkyl chains on the imidazolium cation.

2.2 Fluoro-Anion-Based ILs

The main defect of these halide ILs is that they are very sensitive to the water in air, which prohibits development of further applications. The fluoro-anion ILs (e.g., anion = $[BF_4]^-$, $[PF_6]^-$, $[(FH)_nF]^-$, $[AsF_6]^-$, $[OCOCF_3]^-$, $[OSO_2CF_3]^-$, etc.) are typically air-stable and have a greater potential in many chemical processes.

2.2.1 X-ray Diffraction Single-Crystal Structures

1. ILs with Cations of Different Alkyl Lengths

ILs have shifted the conventional view on ionic molten salts because of their liquid state at room temperature. Coulombic attractive forces in ILs must be diffuse to inhibit or suppress crystallization. Varying the length or degree of branching of the alkyl chains of imidazolium cations can dramatically change their melting points. This has attributed to variations in the rotational freedom of the alkyl chains of the cations and the ability of the cations to pack efficiently (or not) within the crystalline cell. Branching in alkyl substituents can similarly lead to increases in

melting point through restriction of rotational freedom, but can also, conversely, reduce melting points when branching results in enantiomeric mixtures.

Reichert et al. have examined the structure of the solid state imidazonium hexafluorophosphate ([Dmim][PF_6]) ILs with different *N*-alkyl chains by X-ray crystallographic analyses [35]. Figure 5 presents the local structures and ion packing in the crystal structures, in which $[PF_6]^-$ anions contact with imidazolium cation via the H-bonds; however, the length of the *N*-alkyl chains have a remarkable effect on the packing of the ions. When the *N*-alkyl chains are short, $C_n \leq 4$, the $[PF_6]^-$ anions contact not only with the heads (ring) of the cation, but also with the tails (alkyl chains), as shown in Fig. 4a–i. As shown in Fig. 4j–l, $[PF_6]^-$ anions make contact with only the heads of the cation when the chains are longer ($C_n > 4$). From the side views of the cations presented in Fig. 5, it is found that there were several locations of the $[PF_6]^-$ anions above and below the imidazolium heads and in close contact with the C and N atoms of the rings. The direct interactions between the delocalized positive charge of the imidazolium ring and the anion is further indication of the Coulombic nature of ILs based on these ions. Although the electrostatic forces are dominant between cations and anions, the close contacts with a wide angular distribution indicates the C−H. . .F H-bonded interaction. However, as Reichert et al. said, the H-bonded interactions were weak and more Coulombic in nature. Thus, the interactions that are present in the crystal structures of the short chained salts suggest that the forces responsible for packing in a crystalline lattice are predominantly electrostatic or Coulombic in origin. This also suggests that lattice energies can be described by Eq. 4:

$$U_L = 2I\left[\frac{\alpha}{\sqrt[3]{V}} + \beta\right] \tag{4}$$

I is the ionic strength (=1), *V* is the molecular volume (in nm^3) of the lattice, which is equal to the sum of the individualcation (*V*+) and anion (*V*−) volumes, and α and β are empirically derived parameters.

2. ILs with different anions

The ILs containing fluoroanions are air-stable, with a consequent greater potential application in chemical processes. Except for the common ILs with $[BF_4]^-$ or $[PF_6]^-$, some other ILs containing fluoroanions have been reviewed in recent papers by Matsumoto and Xue et al. [36, 37]. The melting points of these fluoroanionic ILs are around freezing point, and thus the solid state structures are important to the understanding of the ILs' behavior. Table 4 lists the crystal structural parameters for the fluoro-containing ILs with typical 1-ethyl-3-methylimidazolium ($[Emim]^+$) cation.

In the crystal, the [Emim][FHF] is layered and it contains the smallest fluorocomplex anion $[FHF]^-$ in the series. The flat imidazolium rings are stacked and arranged in parallel with the interlayer distance of 3.376 Å. In each layer, very short hydrogen bond distances between the H atom of the cation ring and the F

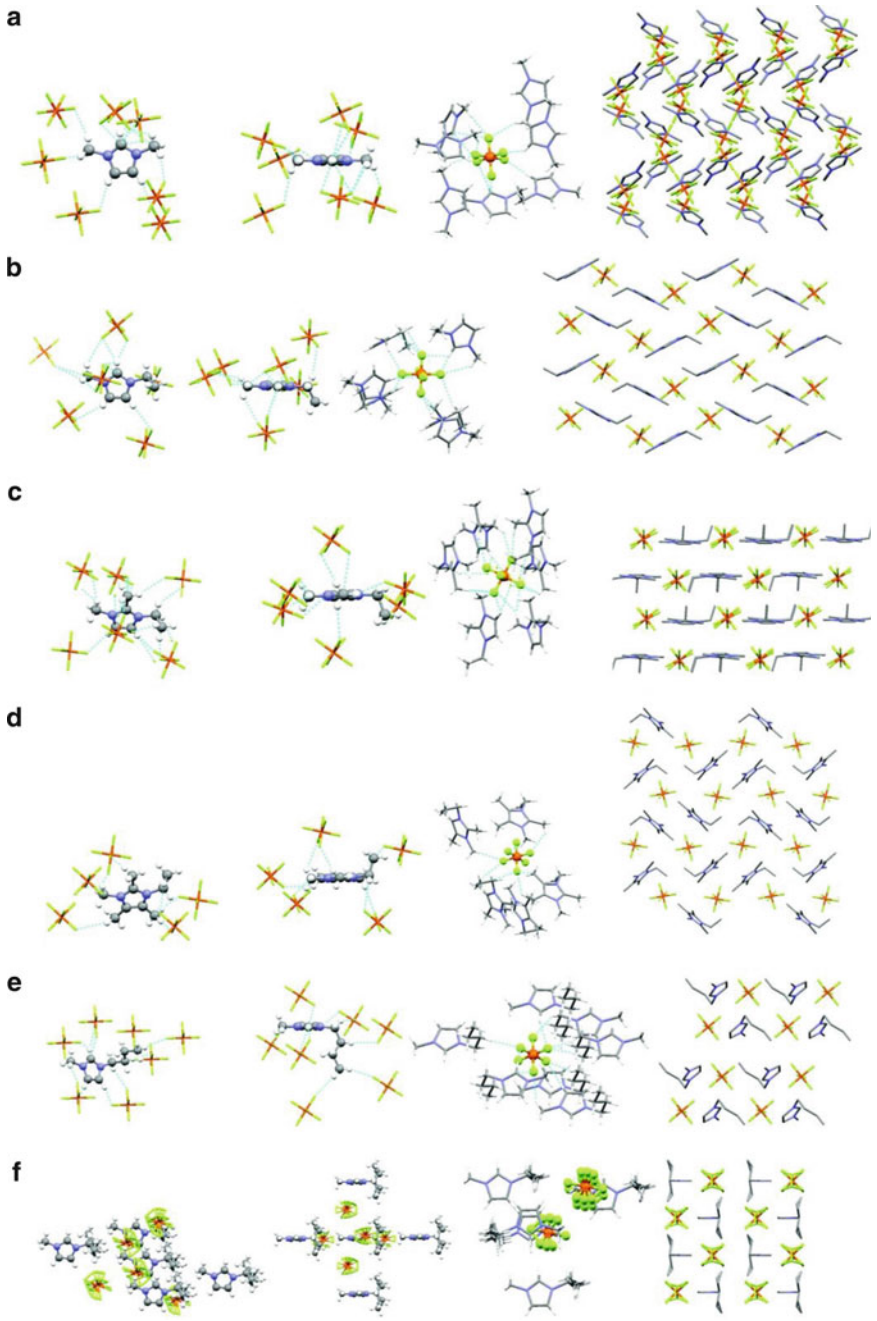

Fig. 5 (continued)

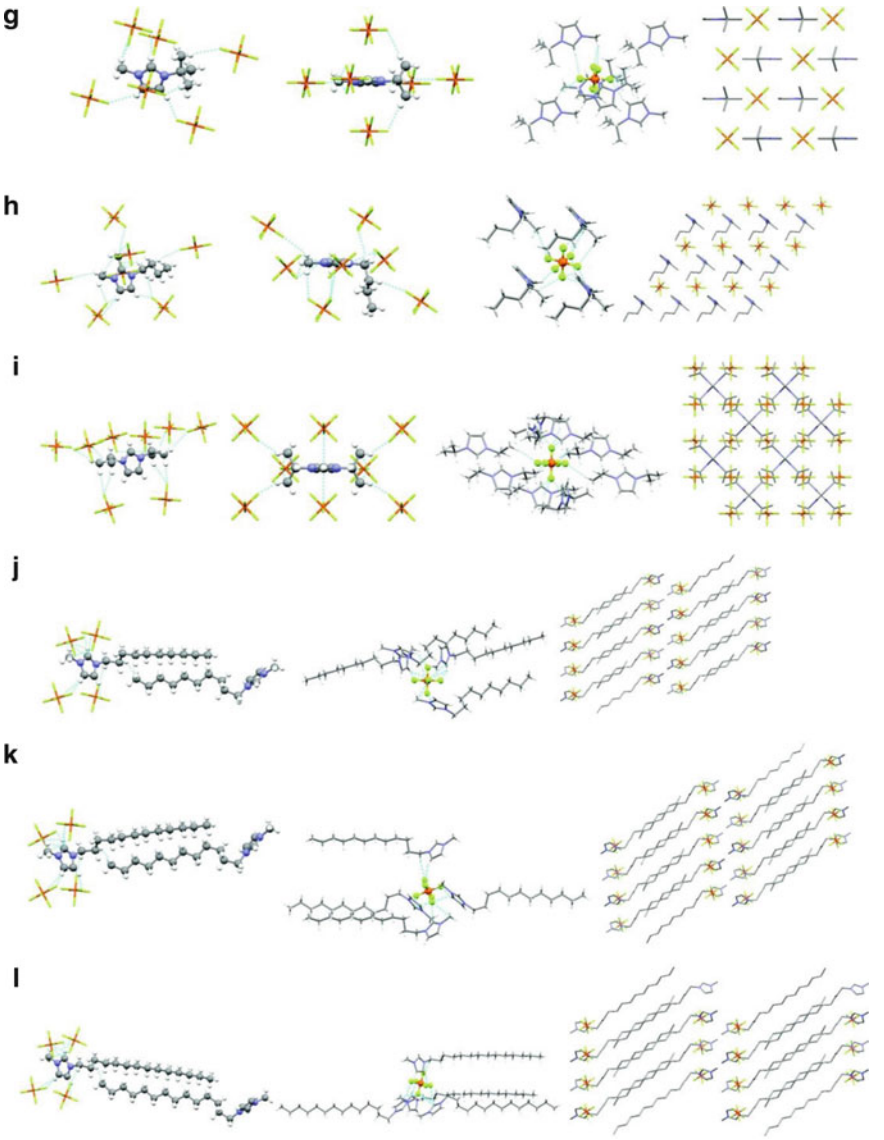

Fig. 5 Local structures and ions packing diagrams of (**a**) [C_1mim][PF_6], (**b**)[C_2mim][PF_6], (**c**) [C_2dmim][PF_6], (**d**)[C_2tmim][PF_6], (**e**) [C_4mim][PF_6], (**f**) [*sec*C_4mim][PF_6], (**g**) [*tert*C_4mim][PF_6], (**h**) [C_4dmim][PF_6], (**i**) [(*iso*C_3)$_2$mim][PF_6], (**j**) [C_{10}mim][PF_6], (**k**) [C_{12}mim][PF_6], and (**l**) [C_{14}mim][PF_6]. The *dashed lines* show the close contacts and H-bonded interactions [35]

Table 4 Cell parameters and melting points of 1-ethyl-3-methylimidazolium ILs with fluoroanions [36]

ILs	Space group	$V(nm^3)$	Z	$D(g{\cdot}cm^{-3})$	$T(K)$
[Emim][BF_4]	$P2_1/c$	0.9068	4	1.450	288
[Emim][FHF]	$P2_1/m$	0.3951	2	1.262	298
[Emim][PF_6]	$P2_1/c$	1.0920	4	1.558	333
[Emim][AsF_6]	$P2_1/c$	1.1234	4	1.775	326
[Emim][SbF_6]	$P2_1/c$	1.1388	4	2.024	283
[Emim][NbF_6]	$P2_12_12_1$	1.1240	4	1.880	272
[Emim][TFSI]·C_6H_6	$P2_1/n$	1.9896	4	1.567	288

atoms of the anion (1.951, 2.166, and 2.226 Å) are observed [38]. In the [Emim][BF_4] IL, $[Emim]^+$ cations form a pillar with the β-carbon of the ethyl group sticking out of the imidazolium-ring plane [39, 40]. The H(methylene)-π interaction sustains the cation–cation interactions with a distance of about 2.86 Å between the H atom in methylene group and the imidazolium ring centroid. [Emim][AsF_6] and [Emim][SbF_6] are isostructural with [Emim][PF_6], whereas [Emim][NbF_6] exhibit a different structure [3, 41]. Figure 6 shows the ion packings in [Emim][AsF_6] and [Emim][NbF_6]. In the [Emim][AsF_6] structure, $[Emim]^+$ cations and $[AsF_6]^-$ anions stack alternately along the β-axis to form pillars. On the other hand, in the [Emim][NbF_6] structure, the anion appears in a zigzag arrangement along the α-axis where the nearest fluorine atoms have a distance of 3.441 Å and the cations adopt a pillar-like stacking along the same axis. H-bonds often play an important role in the melting points of ionic compounds. For salts with fluorocomplex anions, in spite of closer H. . .F contacts in [Emim][NbF_6] than those in [EMIm][PF_6], [EMIm][AsF_6], and [EMIm][SbF_6], the melting points of the former two compounds are much lower than those of the latter three compounds. [Emim][BF_4] also exhibits a low melting point despite relatively strong H-bonds in its lattice. These observations suggest that the strength of hydrogen-bonding is not always a decisive factor in their melting points.

2.2.2 The Structures of Ion Pair and Ion Cluster

1. The Structure of the Ion Pair

It has been verified experimentally that the ions are pairwise in the gas phase [43, 44]. Although in liquid state, the ions are not strictly composed of ion pairs; cations and anions can contact closely due to strong electrostatic attraction. Theoretical calculations have been performed in an attempt to understand the structure of ion pairs and interaction between cation and anion [10, 45].

We have investigated in detail the ion-pair structures of the two typical ILs, [Emim][BF_4] and [Bmim][PF_6], by ab initio DFT calculations [46]. In the [Emim][BF_4] ion pair, $[BF_4]^-$ anion can locate at five positions of cation as shown in Fig. 7. Then the five structures of ethyl-front, methyl-back, back, methyl-front and ethyl-back

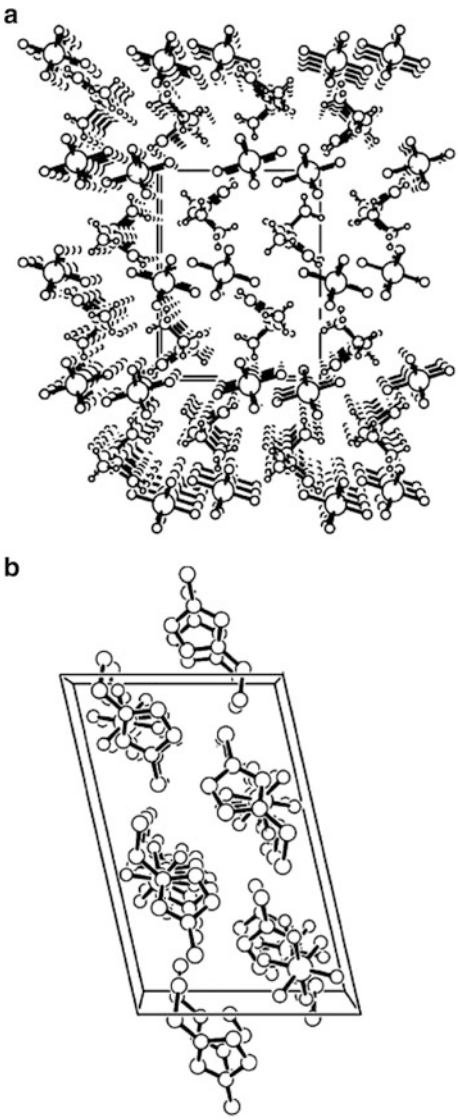

Fig. 6 Ions packing in solid (**a**) [Emim][NbF_6] and (**b**) [Emim][AsF_6] ILs [42]

as initial configurations were optimized at B3LYP/6-31++G** theory level. Finally, the three lowest energy geometries were obtained. The [Emim][BF_4] (I) was obtained from the ethyl-front, methyl-back, and back configurations, in which $[BF_4]^-$ anion moved to the upper part of the ring from the lateral part and located near to the C_2–H group. The [Emim][BF_4](II) was obtained from the methyl-front configuration and $[BF_4]^-$ anion also moved to the upper part of the ring. [Emim][BF_4](III) was obtained from the ethyl-back conformer, but $[BF_4]^-$ anion did not move and only localized near to the C_5–H group.

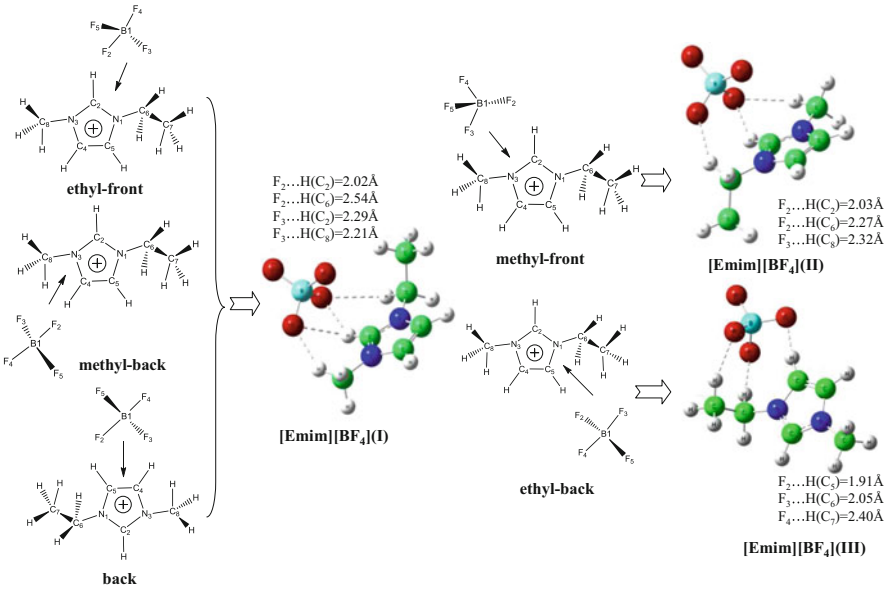

Fig. 7 The optimized structures of [Emim][BF_4] ion-pair when anions are located at five different positions of cation. The *arrows* indicate the initial locations of the anion. The *dashed lines* indicate the H-bonds in these ion pairs

A shallow potential energy well was present when the $[BF_4]^-$ anion localized at the back and the methyl-front of imidazolium ring and experienced the minimal electrostatic attraction to the significant stronger electrostatic attraction due to the essential neutral charge distribution on the $C_{4/5}$ atoms and the positive charge on the C_2 atom. However, when localizing at the ethyl back of imidazolium ring as shown in Fig. 7, it is difficult for the $[BF_4]^-$ anion to move due to steric exclusion derived from the ethyl side chain and the electron repulsion derived from the π-bond between the C_4 and C_5 atoms.

To date, many researchers have discussed the possible interactions between cation and anion and proposed that H-bonds also widely exist in ILs and represent the most explicit interaction besides electrostatic attraction [47–51]. According to the criterion for forming an H-bond – that the distance between H on donor atom and basic acceptor atom, $R_{H\ldots A}$, is less than the sum of their respective van der Waals radii – herein the van der Waals distance is 2.670 Å [36]. There are four F…H H-Bonds to form in [Emim][BF_4](I) as drawn by dashed lines in the right of Fig. 4. Two H-bonds form between the F atoms labeled F_2 and H(C_2) atoms of the ring, and H(C_6) atom of the alkyl chain. The distances are 2.02 and 2.54 Å, respectively. The other two occur between the F_3 atom and H(C_2) atom of the ring, and H(C_8) atom of the alkyl chain. The distances are 2.29 and 2.21 Å, respectively. A very similar H-bonded structure can be found in [Emim][BF_4](II), but there is no H-bond between F_3 atom and H(C_2) atom. When $[BF_4]^-$ anion locates at the ethyl back of imidazolium ring as [Emim][BF_4](III), shown in Fig. 4,

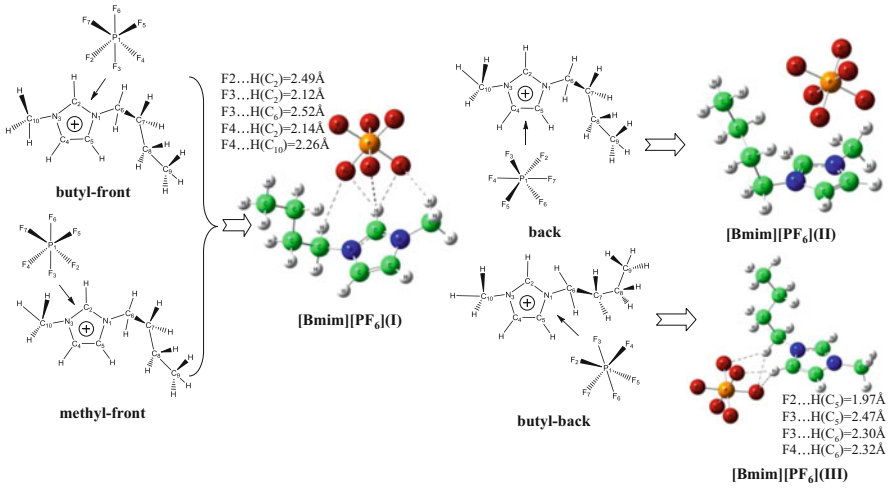

Fig. 8 The optimized structures of [Bmim][PF_6] ion pair with anions located at the five possible different positions around the cation. The *arrows* represent the initial locations. The *dashed lines* indicate the H-bonds in these ion pairs

only two H-bonds form, and one is between the F_2 atom and H(C_2) atom of the ring, and another is between the F_3 atom and H(C_6) atom of the alkyl chain. Their distances are 1.91 and 2.05 Å, respectively.

For the [Bmim][PF_6] ion pair, the similar five initial configurations, butyl-front, methyl-back, back, methyl-front and butyl-back, were optimized at the B3LYP/6-31++G** level. The three lowest energy structures were obtained as shown in Fig. 8. [Bmim][PF_6](I) was obtained from the butyl-front and the methyl-front configurations. [Bmim][PF_6](II) and [Bmim][PF_6](III) were obtained from the back and the butyl-back conformers, respectively. However, no stable point was found at the potential energy surface for the methyl-back configuration. For the back configuration, the $[PF_6]^-$ anion moves above the imidazolium ring and the steric exclusion of the long butyl chain is responsible for the location compared with the shorter ethyl chain on the $[Emim]^+$ cation.

There are five H-bonds in the [Bmim][PF_6](I) ion-pair. One is between the F atom labeled as F_2 of $[PF_6]^-$ anion and the H(C_2) atom of imidazolium ring and the distance is 2.49 Å. Two are between the F_3 atoms and the H(C_2) atom, and the H (C_6) atom of alkyl chain. The distances are 2.12 and 2.52 Å, respectively. The other two are between the F_4 and H(C_2) atoms, and the H(C10) atom of the alkyl chain. The distances are 2.14 and 2.26 Å, respectively. When the $[PF_6]^-$ anion locates at butyl-back, there are four H-bonds as [Bmim][PF_6](III) in Fig. 8. One H-bond can form between the F_2 atom and the H(C_5) of ring, and the distance of 1.97 Å is the shortest. The other three are between two F atoms and H(C_5) and H(C_6) of the alkyl chain, and the distances are 2.47, 2.30, and 2.32 Å, respectively. However, when the $[PF_6]^-$ anion locates at the back of imidazolium ring, the $[PF_6]^-$ anion moves above imidazolium ring to form the [Bmim][PF_6](II) and there is no H-bond to form.

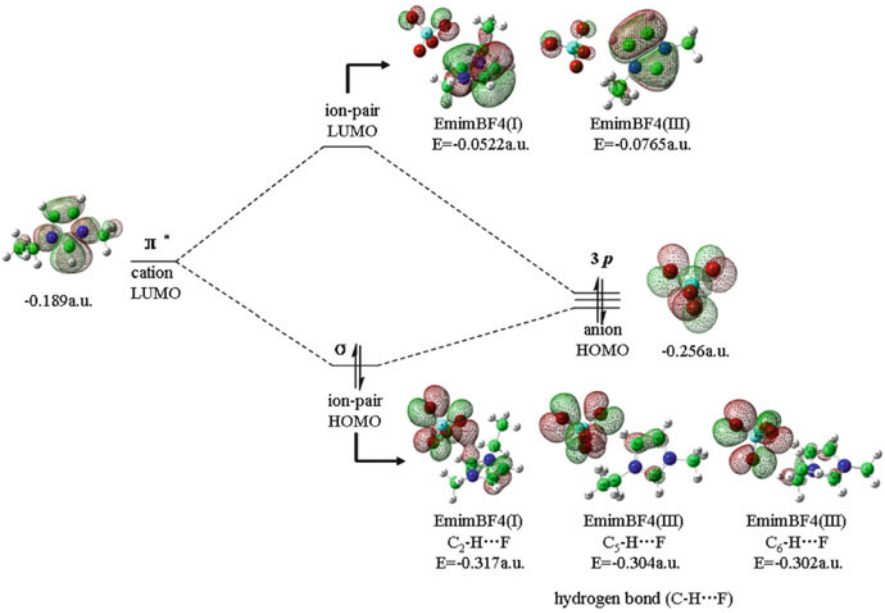

Fig. 9 The orbitals and energies diagram for [Emim][BF_4] ion-pairs. (Due to the same orbital diagram with [Emim][BF_4](I) ion-pair, the [Emim][BF_4](II) ion-pair were not drawn)

2. Understanding the Interaction at Electronic Level

By NBO analysis it was found that in [Emim][BF_4] ion-pairs the occupation on the N_3 orbital always increases, while the occupations on the $\pi_{C2=N1}$ and $\pi_{C4=C5}$ orbitals vary with the positions of anion. In [Emim][BF_4](I) and [Emim][BF_4](II) ion pairs, the occupation on the $\pi_{C2=N1}$ orbital decreases, but on the $\pi_{C4=C5}$ the orbital increases. In [Emim][BF_4](III) ion-pair, the occupation of the $\pi_{C4=C5}$ orbital decreases, and the occupation on the $\pi_{C2=N1}$ orbital exhibits no significant change. Furthermore, the molecular orbitals provide an essential insight into the ion pairs. Figure 9 shows the orbitals and energies for both [Emim][BF_4](I) and [Emim][BF_4](III) ion-pairs. The HOMO of the isolated anion is degradation p orbitals (energy E = −0.256), and the LUMO of the cation is the anti-π (π*) bond orbital (energy E = −0.189). However, in the ion pairs there are not the expected p-π orbital interactions, but the HOMO of the [Emim][BF_4](I) is the highest occupied p orbital of anion and the lowest empty $\pi^*_{(C2-H)}$ orbital of cation, and the LUMO of [Emim][BF_4](I) exhibits an anti-σ (σ*) bond orbital (energy E = −0.0522). In the [Emim][BF_4](III) ion pair, the effective orbital overlap also occurs and the HOMO (energy E = −0.304) and the degradation HOMO-1 (energy E = −0.302) are the highest occupied p orbitals of anion and the lowest empty $\sigma^*_{(C5-H)}$ and $\sigma^*_{(C6-H)}$ orbitals of cation. The σ-type interaction rather than p-π overlap indicates a covalent bonding feature, but the formation requires a stronger intermolecular attraction. The electrostatic attraction drives anion to approach cation, and finally

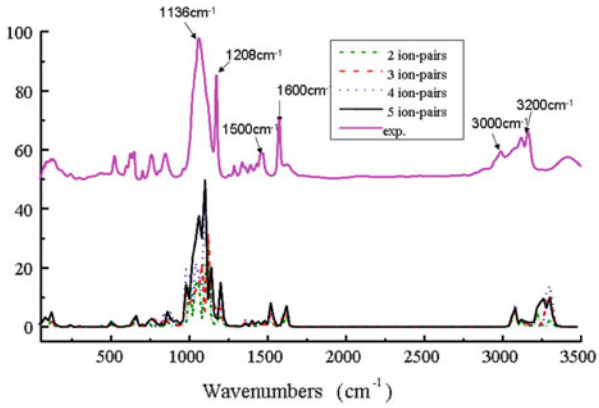

Fig. 10 Measured FTIR spectrum of $[Emim][BF_4]$ at room temperature conditions compared to the vibrational modes of the corresponding ion clusters $([Emim][BF_4])_n$ with n = 2, 3, 4, 5 calculated by DFT at B3LYP/6-31 + G** level (all of the calculated bands were corrected by the factor 0.964–0.967)

locates at the largest positive charge position of the cation. Although the repulsion of the electron between anion and cation increases the total energy, the orbital effective overlap and the partial electrons transfer result in an energetic reduction, and further stabilize the ion pairs.

Obviously from the two classes of ion-pairs with multiple atomic fluoro-anions, we find that more than one H-bonds can form between cation and anion, which is different from ionic liquids with a single atomic anion, like the dialkyimidazolium chloride ([Emim]Cl), and with only one H-bond between cation and anion [45–47].

3. The Structure of Ion Cluster

As reported [52–54], the ions clustering by ionic close contacts reflects the structural arrangement in the bulk phase of RTILs [55]. The clusters may become microscopic models to describe the structures of the bulk ionic liquids or their aqueous solutions. Figure 10 shows an experimental FTIR spectrum of $[Emim][BF_4]$ IL and the calculated IR vibrational frequencies for the $([Emim][BF_4])_n$ ion clusters with different number, n = 2, 3, 4, 5 at B3LYP/6-31 + G** level. The strong agreement on major bands provided the possibility to explore the detailed structural information of $[Emim][BF_4]$ IL, and these experimental vibrations can also be assigned rationally by the structures of these ion clusters.

The band at 3,000–3,500 cm^{-1} is assigned to the symmetric stretches of three C–H bonds of the imidazolium ring. Two weaker peaks around 1,600 and 1,500 cm^{-1} are assigned to the breadths of the rings and the scissors of the alkyl chains, respectively. The peaks around 1,208 cm^{-1} are assigned to the interplanar wagging vibrations of the C–H bonds on rings. The strongest peak occurs around 1,136 cm^{-1} and is assigned to the stretches of B–F bonds of $[BF_4]^-$ anion, while these weak peaks around 750–880 cm^{-1} are the out-of-planar wagging vibrations of the rings.

Structural investigation into the clusters has found that the ion arrangements are ordered and similar to the crystal structure shown by X-ray [40, 42]. The structures of clusters are shown in Fig. 11. It was found that these ions are connected by the H-bonds (dashed lines) together to form a three-dimensional network [47]. In the network, the ion packing is influenced very little by the intramolecular bonding

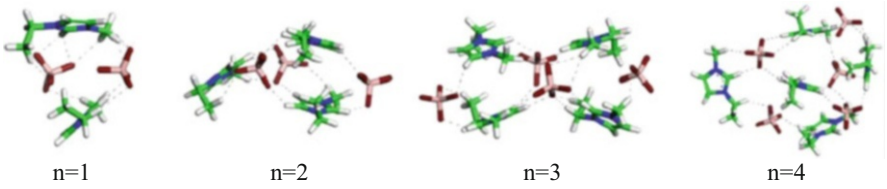

Fig. 11 The ion clusters of $([Emim][BF_4])_n$ with n = 2, 3, 4, 5 by tube fashion. The *dashed lines* denote the forming H-bonds

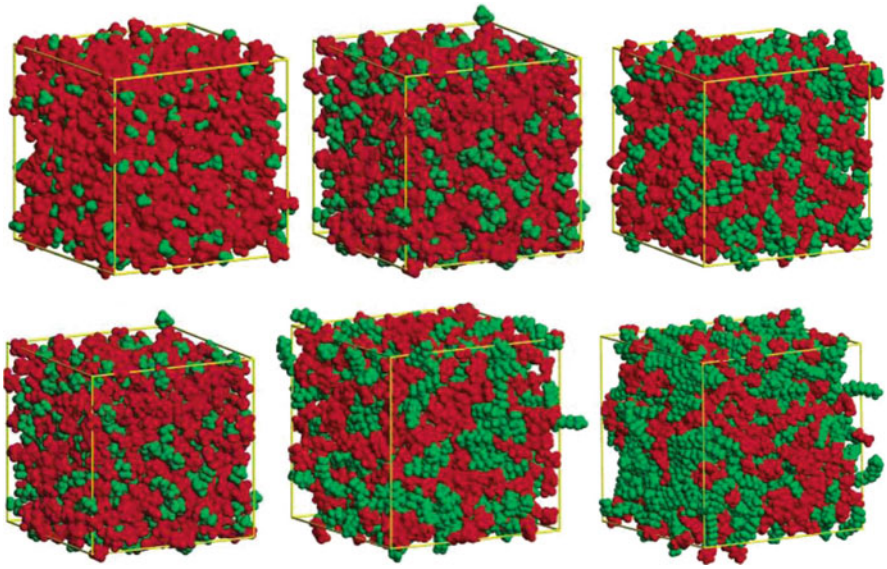

Fig. 12 The nano-clusters observed $[C_n mim][PF_6]$(n = 2,4,6,8,10,12) by molecular dynamic simulation [3]

structures, and the imidazolium cations are arranged in alternative layers and the $[BF_4]^-$ anions are sandwiched between two cations but do not locate above the rings and prefer to be near the C-H groups of rings in the clusters. The cation–cation distance is around 5.10 Å between H(C_2) atom and the imidazolium ring center. No strong interaction between the ring proton and π-electron cloud of the imidazolium ring is observed and the ethyl groups stick out of the imidazolium ring planes (C_2–N_1–C_6–C_7 torsion angle around 74°). $[BF_4]^-$ anions form a pillar with a B. . .B distance of 5.7 Å in two different anions. Neutron diffraction studies on some RTILs indicated that charge ordering endured in the liquid phase.

Larger nano-clusters have been observed in imidazolium-based ILs with alkyl chain length more than 4. Based small-wide-angle X-ray (SWAXS), Hardacre et al. have found low-Q peaks in $[C_n mim][PF_6]$ (n = 4, 6, 8) ILs,which are correlated with the heads (imidazolium rings) of cations and indicate the heads aggregate together [56, 57]. These observations have been supported by molecular dynamic simulation. Figure 12 shows the ion packings of $[C_n mim][PF_6]$ (n = 2, 4, 6, 8, 10, 12)

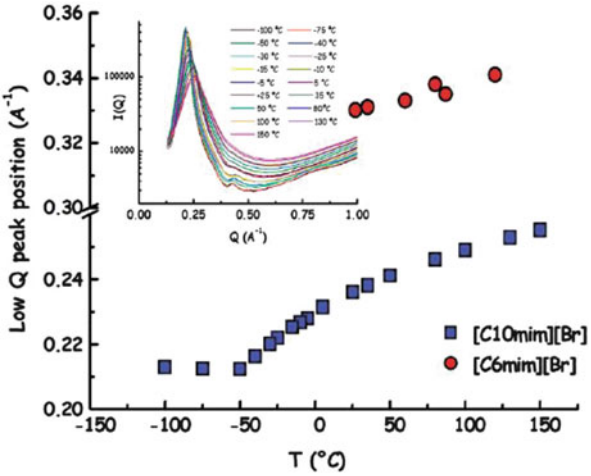

Fig. 13 The changes of low-Q peaks of [C_6mim]Br and [C_{10}mim]Br along with the increasing temperatures from −100°C to 150°C. The inserted shows the SWAXS Q values at different temperatures

ILs observed by molecular dynamic simulation [58]. It can be seen that the ions do not aggregate when connected with short chains (n = 2). When the lengths of the alkyl chains are increased (n = 4, 6, 8), the ions start to aggregate, and the polar domains (red color, the charged anions and imidazolium ring parts) and the non-polar domains (green color, the non-charged alkyl chains) are obvious. When the lengths of the alkyl chains were increased to n = 12, the aggregation is very obvious, and the larger clusters form. In the clusters, the anions and imidazolium rings aggregate together to form the polar domains by charged attraction, and the non-charged long alkyl chains "twist" together to form non-polar domains.

Except for the structural factors, the nano-clusters can be influenced by the temperature, pressure, and concentration in binary systems. Triolo et al. found that the low-Q peaks decrease with increasing temperatures in solid ILs, but the low-Q peaks increase with increasing temperatures in liquid ILs [59]. Figure 13 shows the low-Q peak curve of the [C_6mim]Br and [C_{10}mim]Br ILs with increasing temperatures [60]. It can be seen that the low-Q peaks of [C_{10}mim]Br decrease with increasing temperatures in the −100~−50 °C range, but the low-Q peaks increase linearly with increasing temperature in the −50~150°C range. Nevertheless, over the complete temperature ranges the low-Q peaks are very low, indicating that the nano-clusters exist throughout, even at a temperature as high as 150 °C, as shown by the Q values obtained at different temperatures. For [C_6mim]Br the situation is not the same. The low-Q peaks increase linearly with temperature, increasing over the 0~150 °C range, but the change is not obvious.

In general, the ions in the bulk phase are not randomly packed and the electrostatic force, van der Waals, and H-bonds rationalize the preferable arrangement.

3 Non-covalent Interaction in ILs

3.1 Binding Energy of Ion Pair

S. Zahn et al. compared the binding energies of one [Mmim]Cl with the NaCl ion pair by the symmetry-adapted perturbation theory (SAPT) method, considering different contributions in analogy to a multipole expansion (Fig. 14) [61]. For the NaCl (red diamonds in Fig. 14a) the dispersion term is negligible, whereas this contribution is comparable in magnitude to the induction term for the two conformers of the ionic liquid pair [Mmim]Cl (blue and green diamonds). The total energy of NaCl consists of only electrostatic, exchange, and induction contributions (see Fig. 14b; the curve with red squares almost exactly matches the curve with diamonds). We can make another interesting observation concerning the minima. Whereas the NaCl features the minima for all curves exactly at the equilibrium distance (at zero, see black dotted vertical line), this is, surprisingly, not the case for the [Mmim]Cl pairs (see black arrows). This means that the equilibrium distance is not exclusively determined by the most important attractive force, namely, the electrostatic interaction.

This finding demonstrated that the ions interact in the repulsive region of electrostatic potential only if one considers that the hypothetical potential consists of electrostatic and exchange terms. This implies that ILs are not as ionic as one may naively imagine. Different contributions partly compensate each other, resulting in a very shallow potential energy curve. Consequently the system is highly flexible and liquid like, and is also able to adjust easily to different situations, which might also explain the good solvating properties of ILs.

Table 5 also lists the binding energies of $[Emim]^+$-based complexes with different counter-anions. The binding energies follow the trend $[CF_3CO_2]^- > [BF_4]^- > [CF_3SO_3]^- > [Tf_2N]^- \sim [PF_6]^-$. However, the experimental properties (melting point, density, self-diffusion coefficient, and molar conductivity) have no defined correlation with these binding energies, which indicates that many properties of RTILs are not determined just by interaction energy.

Melting point is the basic property of ILs and reflects the molecular packing and interactions of cations and anions. A rough correlation of melting points (T_m, K) and binding energies (E, kJ · mol^{-1}) for dialkylimidazolium chloride, bromide, dialkylimidazolium tetrafluoroborate, and dialkylimidazolium hexafluorophosphate ILs is shown in Fig. 17 [47]. A linear relationship was assumed for these ILs and their melting point decrease when the sizes of the *N*-alkyl side chains increase. Seven species of the Cl^- and Br^- series, except for [Pmim]Br, were correlated and the linear relationship is very pronounced. The melting points range from 300 to 400 K while the interaction energies lie between −375 and −320 kJ · mol^{-1}. A similar trend was observed for four species of the $[PF_6]^-$ series, but the linear relationship is very gross. For four species of $[BF_4]^-$, the linear relationship between melting points and interaction energies is also pronounced, but the difference between successive melting points is much greater than the difference between successive energies:

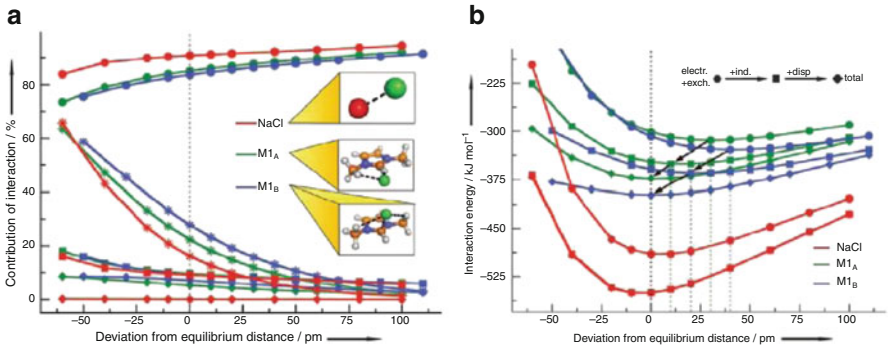

Fig. 14 (**a**) Contributions of different interactions to the total attractive (electrostatic + induction + dispersion) interaction energy. (**b**) Plot of the interaction energy versus distance [61]

Table 5 Binding energies and properties of ILs

	E^a	$M_p{}^b$	ρ^c	D^d	$\Lambda_{imp}{}^e$	$\Lambda_{NMR}{}^f$	$\Lambda_{imp}/\Lambda_{NMR}{}^g$
[Emim][CF_3CO_2]	−89.8	−14	1.22	3.23	0.63	1.25	0.51
[Emim][BF_4]	−85.2	11	1.20	2.72	0.69	1.04	0.66
[Emim][CF_3SO_3]	−82.6	−9	1.30	3.02	0.64	1.10	0.58
[Emim][Tf_2N]	−78.8	−15	1.44	4.75	1.10	1.82	0.60
[Emim][PF_6]	−78.4	62	1.37	1.21	0.31	0.46	0.68
[Py][BF_4]	−82.8	26	1.44	3.91	0.94	1.44	0.66
[$(C_2H_5)(CH_3)_3N$][BF_4]	−84.6	19	1.39	2.34	0.61	0.91	0.67

[a]Energies in kcal/mol
[b]Melting points (°C)
[c]Density ($g{\cdot}cm^{-3}$)
[d]Self-diffusion coefficient (cation + anion) at 298 K (10^{-7} $cm^2{\cdot}s^{-1}$)
[e]Molar conductivity obtained from impedance measurement ($S{\cdot}cm^2{\cdot}mol^{-1}$) at 298 K
[f]Molar conductivity obtained from ion diffusivity measurement by NMR ($S{\cdot}cm^2{\cdot}mol^{-1}$) at 298 K
[g]Ratio of $\Lambda_{imp}/\Lambda_{NMR}$

the melting points are in a range 400–200 K while the interaction energies are between −350 and −340 kJ · mol^{-1}. Therefore, it is indicated that the more atoms the anions include, the more complicated are the interactions between cations and anions.

Molar conductivity is an important property of RTILs for their application as electrolytes for electrochemical devices. S. Tsuzuki et al. [18] reported the measurement of the molar conductivity of RTILs composed of $[Bmim]^+$ cation. They found that the molar conductivity obtained from impedance measurement (Λ_{imp}) is smaller than that obtained from ion diffusivity measurement by NMR (Λ_{NMR}). They pointed out that the $\Lambda_{imp}/\Lambda_{NMR}$ value provides useful information on the ionic dissociation/association dynamics in the ionic liquid (Table 6). They reported that the $\Lambda_{imp}/\Lambda_{NMR}$ values of RTILs composed of $[Bmim]^+$ follow the order $[PF_6]^- > [BF_4]^- > [Tf_2N]^- > [CF_3SO_3]^- > [CF_3CO_2]^-$. A small $\Lambda_{imp}/\Lambda_{NMR}$ value shows that an ion prefers to move with a counterion. $\Lambda_{imp}/\Lambda_{NMR}$ is an important parameter

Table 6 Experimental spectroscopic studies on interactions and H-bonds in some typical ILs

Ionic liquid[a]	Spectra	H-Bond[b]	HBDA(α)[c] [65–67]	ΔE[d] [18, 47]	Mp[e]	Td[f]
[Dim]Cl	X-Ray, IR[68],NMR [69],Neutron[70]	C–H···Cl(Br, I)	0.44[g]	378.03	84	285
[Dim][BF_4]	X-Ray, IR[71]	C–H···F	0.61	356.47	11	412
[Dim][PF_6]	X-Ray[72], Neutron [70, 73],IR	C–H···F	0.64	319.00	10	375
[Dim] [OSO_2CF_3]	X-Ray[74], NMR[13], IR[75]	C–H···O, C–H···F	0.60	345.60	−9	140
[Dim] [$OCOCF_3$]	X-Ray, NMR[13]	C–H···O, C–H···F	0.56	375.72	−14	150
[Dim][Tf_2N]	X-Ray[76], THz, IR [77], Neutron	C–H···N, C–H···F, C–H···O	0.66	313.60	−15	455
[Pyr][Tf_2N]	X-Ray, Raman[78]	–	0.48	–	26	–
[(C_4H_9) (CH_3)$_3$N] [Tf_2N]		–	0.47	–	19	–

[a][Dim]$^+$ represents the 1,3-dialkylimidazolium cation, [Pyr]$^+$ represents the pyridinium cation
[b]Possible H-bonds between cation and anion in crystal and liquid phase
[c]H-bonded donation abilities (only for [Bmim]$^+$ cation)
[d]Average binding energies were calculated by the DFT and MP_2 methods (only for [Emim]$^+$ cation)
[e]Melting points (°C)
[f]Measured thermal decomposed temperature (°C) (for [Emim]$^+$ cation)
[g]Measured in supercooled state

for designing highly conductive ionic liquids. The RTILs composed of round-shaped anions ([PF_6]$^-$ and [BF_4]$^-$) have larger $\Lambda_{imp}/\Lambda_{NMR}$ values than those composed of the other rod-shaped anions. The round-shaped anions dissociate and associate with cations more easily in the RTILs. The interaction energy of the [Emim]$^+$ complex with [PF_6]$^-$ anion(-78.4 kcal $\cdot$ mol^{-1}) is smaller than that of the [BF_4]$^-$ complex (-85.2 kcal $\cdot$ mol^{-1}). The [BF_4]$^-$ binds with [Emim]$^+$ more strongly than the [PF_6]$^-$, which well explains the smaller $\Lambda_{imp}/\Lambda_{NMR}$ value for [Bmim][BF_4] than that for [Bmim][PF_6]. The interaction energy of complexes with [Tf_2N]$^-$, [CF_3SO_3]$^-$, and [CF_3CO_2]$^-$ are $^-$78.8, $^-$82.6, and -89.8 kcal $\cdot$ mol^{-1}, respectively. The order of $\Lambda_{imp}/\Lambda_{NMR}$ of three RTILs composed of [Bmim]$^+$ and the rod-shaped anions coincides with the reverse order of the magnitudes of the interaction energies of the [Emim]$^+$ complexes.

Comparison of the calculated interaction energies of the ion pairs and experimental $\Lambda_{imp}/\Lambda_{NMR}$ values of RTILs suggests that three factors play important roles in determining the $\Lambda_{imp}/\Lambda_{NMR}$ value: (1) RTILs have large $\Lambda_{imp}/\Lambda_{NMR}$ values if the interaction between cation and anion is small; (2) RTILs that consist of round-shaped ions have large $\Lambda_{imp}/\Lambda_{NMR}$ values – probably the round shape of the ions enables a high mobility of the ions in RTILs; (3) RTILs have large $\Lambda_{imp}/\Lambda_{NMR}$ values if the orientation dependence of the interaction is small. A large anisotropy of the interaction would probably decrease the mobility of the ions.

3.2 Hydrogen Bonds

3.2.1 Structural Characteristic of H-Bonds

The particular resonance structure and high π electronic delocalization of the imidazolium cation result in large positive charges on the C_2–H, C_4–H and C_5–H groups that are the main interactive positions with anion [45, 62]. As discussed previously, H-bonds are explicit non-covalent interactions in ILs, but are not the same with different anions. For the anions with one atom, like the [Emim]Cl ion pair as shown in Fig. 15a, only one C–H. . .Cl H-bond forms between cation and anion. For anions with multiple atoms, like [Emim][BF_4] in Fig. 15b, more than one C–H. . .F H-bond forms between cation and anion [47].

The electronic structure investigation found that the HOMO of Cl^- can interact with the LUMO of the cation to form a σ-type orbital overlap such that the Cl^- anion can localize near to the C_2–H group as shown in the [Emim]Cl ion pair [47, 63]. A similar σ-type orbital overlap can also be found in the [Emim][BF_4] ion pair. Therefore the orbital overlap results in the significant energy reduction, further rationalizing the preferable location of the anion.

3.2.2 Evidence of H-Bonds in ILs

Many ILs have been studied by experimental spectroscopy (IR, Raman, NMR, neutron scattering, etc.) and results have indicated that the ions can array orderly over a larger range of temperatures [36]. The earliest X-ray studies found that there existed a discrete H-bond in halide-based ILs (anions = Cl^-, Br^-, and I^-) [64]. The evidence from X-ray and IR spectra from [Emim]Cl IL have demonstrated unambiguously that the H-bond not only exists but the is also most explicit interaction between the ions (Table 6). The Cl^- anions are located with the cation by H-bonds rather than at random.

For the fluoro-anion-based ILs (e.g., anion = $[BF_4]^-$, $[PF_6]^-$, $[(FH)_nF]^-$, $[AsF_6]^-$, $[OCOCF_3]^-$, $[OSO_2CF_3]^-$, etc.), X-ray studies have indicated that F atoms of the anions can form C–H. . .F H-bonds with the imidazolium cation, in particular C–H_2, C–H_4 and C–H_5 groups on the ring as listed in Table 6 [36]. NMR studies have also provided structural depictions for [Mmim][PF_6] IL [72], in which the asymmetric unit contains one ion-pair, and the imidazolium cations form a weakly C–H. . .π hydrogen-bonded zigzag chain along the (0 0 1) direction. The $[PF_6]^-$ anions are located between these chains and make closest contacts with the hydrogen atoms of the cation. The liquid phase of the [Dim][PF_6] shows a similar structure to the crystal state by neutron diffraction [79].

In crystal structures of dialkylimidazolium salts containing $[OSO_2CF_3]^-$ or $[OCOCF_3]^-$ anions, for example [Bmim][OSO_2CF_3] IL, the imidazolium ring and the -SO_3 group of the anion are connected by the C–H. . .O H-bonds to form a two-dimensional NaCl-like arrangement in each layer, and the butyl chain of the

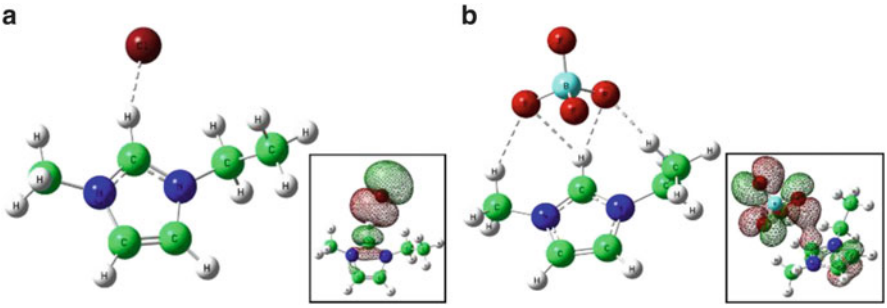

Fig. 15 The H-bond denoted by a *dashed line* in imidazolium-based ionic liquids. (**a**) The optimized geometry and molecular orbital of [Emim]Cl ion pair by DFT method. (**b**) The optimized geometry and molecular orbital of [Emim][BF_4] ion pair

cation and the -CF_3 group of the anion protrude out of the layer in the same direction. Therefore, this structure contains a layer of butyl and -CF_3 groups sandwiched between the two layers. In the liquid state this more ordered structure is not obvious, but except for the C–H. . .O H-bonds between the cation and the -SO_3 group of the anion, the -CF_3 group of the anion can connect with the other cation by C–H. . .F H-bonds [39]. For [Dim][Tf_2N] ILs, both crystallographically distinct [Tf_2N]$^-$ anions adopt a *cis*-conformation [80]. The crystal lattice of [Dim][Tf_2N] consists of alternating two-dimensional sheets with an –AA–B–AA– pattern.

Neutron diffraction studies on some RTILs have indicated that charge ordering endures in the liquid phase. In the [Mmim]Cl and [Mmim][PF_6] salts, the molecular packing in the first two or three solvation shells are similar both in the crystal and in the liquid, although the atomic distances are altered in the liquid [70, 73]. In comparison, the [Mmim][Tf_2N] salt showed smaller charge ordering [79] because of the diffuse charge density and larger size of the [Tf_2N]$^-$ anion. Moreover, its liquid structure is poorly correlated to its crystal structure [80]. This was attributed to the conformational flexibility of the [Tf_2N]$^-$ anion [79, 80]. Nevertheless, it remains clear that ILs form "quasimolecular" structures through three-dimensional H-bonded networks. The network is maintained to a great extent even in solutions having low dielectric media, making the RTILs highly organized media.

Further evidences have demonstrated that by substituting a hydrogen atom for a -CH_3 group, which is incapable of H-bond formation, the bands associated with stretches or bends of H-bonds disappear completely. R. Ludwig et al. [48, 76, 77] had demonstrated that the bands that relate to H-bonds disappeared in [Emim][Tf_2N] IL when the proton atoms on the imidazolium-ring were replaced by -CH_3 groups. With the increased abilities and strengths of H-bonds, the [Tf_2N]$^-$ anion was found in the *cis* conformation. Switching off these local interactions leads to the energetically favored *trans* conformation. These structural effects caused by H-bonds should have significant influence on IL properties, such as melting points and viscosities, as discussed later. Moreover, the vibrational frequencies of H-bonds themselves can be observed directly by far-IR spectrum even for the

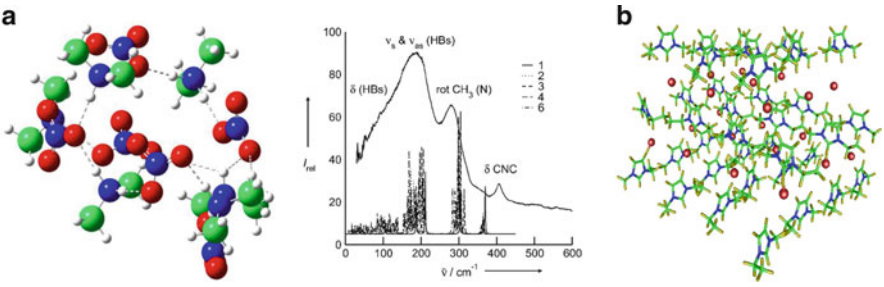

Fig. 16 The ion clusters and the local H-bonded network in ILs. (**a**) The ion cluster of dimethylammonium nitrate (DMAN) and the measured low-frequency vibrational FTIR spectrum of at 353 K compared to the vibrational modes of the corresponding PIL clusters $[(DMA)(NO_3)]x$ with x = 1, 2, 3, 4, and 6 calculated by DFT at the B3LYP/6-31 + G* level of theory [77]. (**b**) Schematic representation of H-bond network IN [Emim]Cl IL. All of the H-bonds were are denoted by *dashed lines* [85]

complicated [Dmim][Tf_2N] IL as listed in Table 6. Wavenumbers above 150 cm^{-1} were assigned to intramolecular bending modes of cations and anions in the ILs, and the wavenumbers below 150 cm^{-1} were assigned to the bending and stretching vibrational modes of H-bonds [81].

The solvent properties of these ILs have also been investigated using chromatographic techniques [82, 83]. It is generally found that the ILs may be considered to be polar phases with the solvent properties being largely determined by the ability of the salt to act as an H-bond donor and/or acceptor. Table 1 lists the H-bonded donation abilities (HBDA, α) to denote qualitatively the acidity of ionic liquids. The α of the pyridinium-based and the quaternary amino ILs are obviously smaller than that of the imidazolium cation, which indicates that the interactions of H-bonds are not remarkable in these ILs.

3.2.3 Local H-Bonded Network

As previously described, involved in the interactions of many ions in bulk ILs, the forming H-bonds can be extended to form a three-dimensional network as in liquid water [84]. The network can even be observed on a smaller nanometer scale domain or in an ionic cluster in which non-homogeneity of local structure is found in ionic liquids. A network of ammonium nitrate IL (ANILs) is shown in Fig. 16, in which cations and anions are connected together by H-bonds (O atom as acceptor on anion and N–H as donor on cation) [48].

Crystallographic studies had also found that the H-bonded networks exist below melting points or at glass state temperatures in many ILs [35, 36, 86]. A remarkable three-dimensional H-bonded network of the [Emim]Cl [86] from X-ray and DFT calculations is shown in Fig. 16b, in which the asymmetric unit contains four $Emim^+ \ldots Cl^-$ ion pairs. The $[Emim]^+$ ions cluster in four distinct layers

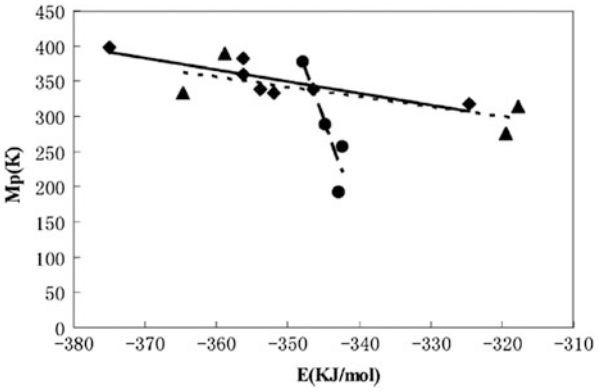

Fig. 17 The correlation of melting points and interaction energies for dialkylimidazolium ionic liquids: Cl and Br salts series (*filled triangles*); [BF_4] salts series (*filled circles*); and [PF_6] salts series (*filled diamonds*) [62]

perpendicular to the *c* axis. Similarly, the arrangement of Cl^- anions is a layered one. Each Cl^- interacts with three $Emim^+$ cations and each $[Emim]^+$ is associated with the three nearest Cl^- ions. The distance from Cl^- to a ring carbon atom averages 3.55 Å. The Cl^- anions are situated in H-bonded positions rather than randomly. In the [Bmim][PF_6] IL, the cations form an H-bonded zigzag chain motif via methyl hydrogen atoms and π-electrons, and $[PF_6]^-$ anions are located between these chains with closest contacts with the methyl hydrogen atoms. Such connection results in the formation of an H-bonded network [72, 87].

Furthermore, molecular dynamical calculations have proved that ions clusters, when viewed over the course of a typical simulation (generally several nanoseconds), remain locked in a local place and the *cations* and *anions* cease to behave as discrete units but act rather as larger supermolecules, H-bonds being responsible for the spatial heterogeneity [52, 88, 89]. Experimental optical Kerr effect spectroscopy [90] also demonstrated the occurrence of heterogeneous domains in 1,3-dialkyl imidazolium salts. The translational and rotational motion of these larger units and their interactions with neighboring molecules explain the high experimental viscosities [91].

4 Effect of Structure on Application of ILs

4.1 Extraction and Separation

Some ILs have been used as solvents in separation processes due to their recovery and recycling properties. Rogers et al. [92] have reported the partition of substituted-benzene derivatives between water and the hydrophobic [Bmim][PF_6]. Their studies

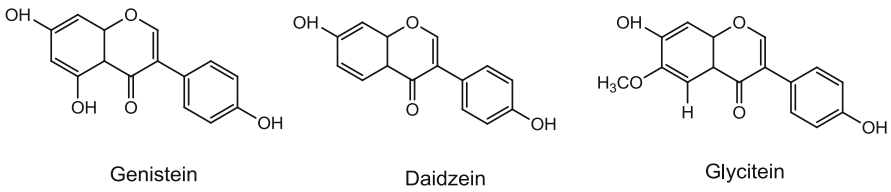

Fig. 18 Soybean isoflavone aglycone homologues

have included the removal of sulfides [93] and nitrides [94] from diesel and gasoline, the separation of aromatics from aliphatics [95], and the removal of pollutants (e.g., phenols, dyes, organic acids) from water, and they have demonstrated the abilities of ILs [94, 96, 97].

Some natural bioactive homologues with high structural similarity have been effectively separated by ILs. Cao et al. [97] have shown that ILs can be used to separate the soybean isoflavone aglycones, known as genistein, daidzein, and glycitein, as shown in Fig. 18. Furthermore, we investigated the interactive mechanism and found that ILs can form H-bonds with the homologues, but the magnitudes of interactions decrease in the order genistein > daidzein > glycitein, which was consistent with the distribution coefficients [98].

Another example is to separate the α-tocopherol from the four tocopherol homologues. The four homologues have different H-bonded acidities resulting from their structural differences in the number and position of methyl groups on the chromanol head. [Bmim]Cl, [Bmim][CF_3SO_3], and [Bmim][BF_4] ILs can extract α-tocopherol successfully from biphasic material in the order [Bmim][BF_4] < [Bmim][CF_3SO_3] < [Bmim]Cl under the same conditions [96]. This order is consistent with the that of these ILs' hydrogen-bond basicity strength [99]. This phenomenon further disclosed that the selectivity was based on the hydrogen-bonding interaction between ILs' anion and the -OH group on the tocopherols.

4.2 Dissolution of Cellulose

Biocompatible composites generated from renewable biomasses are regarded as promising materials that could replace traditional polymers and reduce global dependence on fossil fuels [100–102]. Rogers et al. applied ILs as green solvents to dissolving cellulose, which has opened up a new area for application of ILs in bio-energy [103]. The experiments have proved that many ILs, such as [Bmim]Cl, [Amim]Cl, [Emim]Cl, [BMPy]Cl, [Bmim][OAc], [Amim][OAc], [Emim][OAc], [Emim][XS], and [$N_{111}C_2H_4OH$][OAc], can effectively dissolve the biomass from wood, bagasse, wool, silk, chitin, etc. [100, 103–106]. Experiments and calculations have both proved that the formation of H-bonds between ILs and biomolecules play crucial roles in the dissolving process [107–109]. By means of ^{13}C and $^{35/37}Cl$ NMR relaxation measurements, R. C. Remsing et al. demonstrated

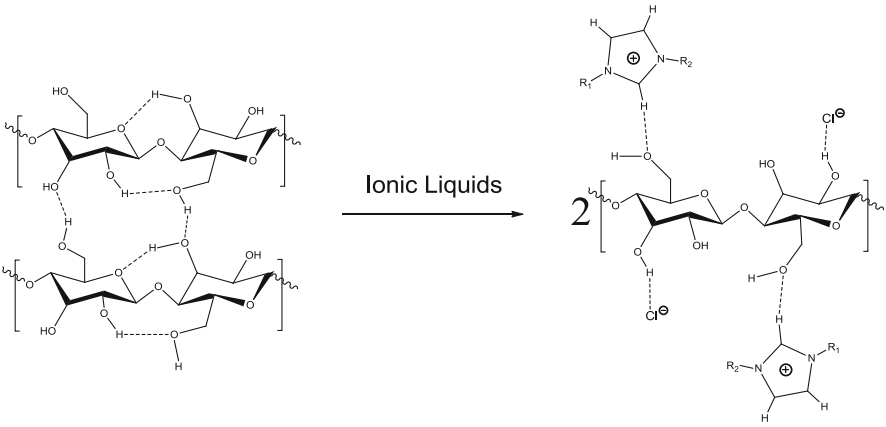

Fig. 19 A proposed mechanism of dissolution of cellulose in ionic liquids. *Dashed lines* show the hydrogen bonds

conclusively that the solvation of carbohydrates by $[C_4mim]Cl$ involves stoichiometric H-bonding between the hydroxyl protons of the cellulose and the chloride ions of the IL. There may be two steps for the dissolution; the first is to break the H-bonds between anions and cations, then the active chloride anions interact with the hydroxyl groups of cellulose by forming H-bonds. It is also thought that $[C_4mim]^+$ cations may possibly form H-bonds with cellulose and play a non-negligible role in the dissolution process.

Figure 19 showed the proposed dissolution mechanism of cellulose in ILs, and how the oxygen atoms and hydrogen atoms of the –OH groups on cellulose form electron donor-acceptor complexes. The anion can combine with hydrogen atoms of cellulose by H-bonds, whilst the imidazolium cation interacts with the oxygen atoms by hydrogen bonding. Comparing with water, we found that the binding energies of the H-bonds between cellulose and ILs are three times stronger than that between cellulose and water, indicating that cellulose is more easily dissolved in [Emim][OAc] [109]. The presence of water in the IL was shown to decrease significantly the solubility of cellulose, presumably through competitive hydrogen-bonding to the cellulose microfibrils which inhibits solubilization. This phenomenon can also corroborate that hydrogen bonding is a key interaction in the dissolving process of cellulose in ILs.

The increasing basicity of the anion resulting in the higher solubility of biomass is also in agreement with the H-bonding mechanism. C. S. Pereira recently reported that a class of biocompatible and biodegradable cholinium-based ILs, the cholinium alkanoates, showed a highly efficient and specific dissolution of the suberin domains from cork biopolymers. They found that the cholinium alkanoates of increasing alkyl chain length (ethanoate, butanoate, hexanoate) showed augmented dissolution efficiency since the basicity of the anion increases with chain length [110]. It indicates clearly that the H-bond basicity of the solvent system is essential for the dissolution of cellulose.

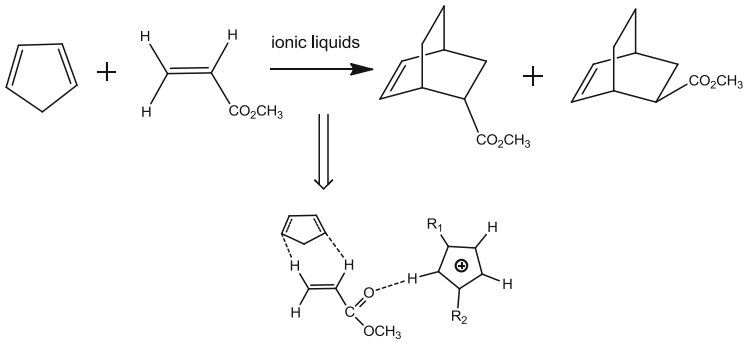

Fig. 20 Diels–Alder reaction by ILs catalysis and the H-bonds (Lewis acid) between imidazolium cation with the carbonyl oxygen of methyl acrylate

4.3 As Catalyst

Diels-Alder cycloaddition reactions have been explored using various ILs substituting for water. The reaction of cyclopentadiene with methyl acrylate and methyl vinyl ketone in IL is shown in Fig. 20 [111]. The studies have found that many ILs can influence the selectivity of the *endo*/*exo*. The theoretical investigation had demonstrated that the ability of the imidazolium cation to act as H-bond donor is responsible for the selectivity. The formation of H-bonds from the cation to dienophile is a Lewis acid–base interaction, as it is well known that Lewis acid catalysts can have a dramatic effect on both the rates and selectivities of Diels–Alder reactions [112].

4.4 Gas Absorption

Studies have shown that many environmental pollution gases, such as CO_2, SO_2, and NH_3, can dissolve freely in ILs [25, 113–115]. The absorption of CO_2 in [Bmim][PF_6] reaches a mole fraction of 0.6 at 25°C and 8.0 MPa [116], and [Bmim][BF_4] and [TMG][BF_4] ILs can absorb 1–2 mole SO_2 per mole of IL reversibly at the ambient pressure and temperature [117].

Figure 21 shows a physico-absorptive mechanics of CO_2 in [Bmim][PF_6] IL. When CO_2 molecules enter the bulk phase of the IL, the O atoms of CO_2 form H-bonds with C–H groups of the imidazolium-ring, and C atoms (with positive charges) can be attracted by anions due to electrostatic interaction. The line-like nonpolar structure of CO_2 is thus changed to give a polar molecule (the angles of the ∠O–C–O are distributed between 175 ~ 178° according to ab initio molecular dynamic calculations, so the change of CO_2 structure results in easier absorption in ILs. The theoretical studies have also indicated that the "spontaneously forming cavities" by H-bonds are vital to accommodate CO_2 and

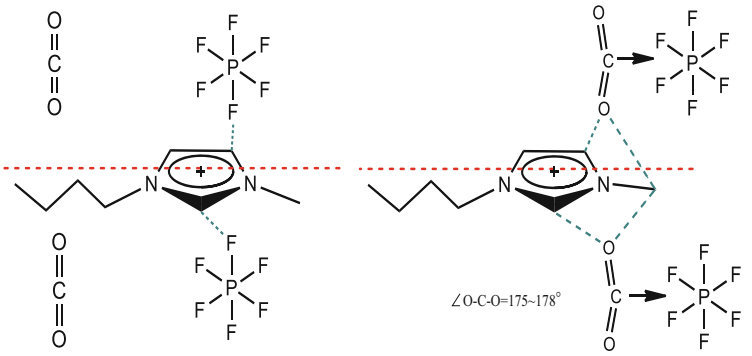

Fig. 21 Proposed mechanics of CO_2 absorption in ILs. The relative positions and the H-bonds change when CO_2 accommodates into the IL physically. *Red dashed lines* show the relative position and *green dashed lines* show the hydrogen bonds. *Arrows* show the electrostatic interactions

SO_2 molecules when they enter the bulk of ILs [118, 119]. However, particularly Ludwig et al. reveal that the experimentally observed "anomalous" temperature dependence of CO_2 in ILs is not due to cavity effects but is caused by attractive solute–solvent interactions. The contribution of the van der Waals interactions is found to dominate [120, 121].

5 Perspective

In the past two decades, explorations of ILs have experienced a fast development and the knowledge base of interdisciplinary data is rapidly being generated for ILs. This will fuel innovative ideas to take these liquids far beyond the realm of mere solvent. However, due to the complications and diversities in ILs' family, it is very difficult to clarify all of the structural factors exerting effects on their properties.

The molecular interactions between ions depend on their geometry and charge distribution. Unlike in simple salts, the interactions are controlled by long-range Coulombic forces between the net charges of the ions. As for ILs with molecular ions, their bulky size and asymmetric charge distribution softens the Coulombic forces and generates highly directional interactions of shorter range. Therefore, almost all studies on the structures of ILs have involved the non-covalent interactions between cations and anions. In most ILs, in particular imidazolium-based ILs, the H-bonds present the structural characteristics and form the three-dimensional local network to connect the discrete ions. The melting points, viscosity, hydrophilic and hydrophobic properties, gas absorption, dissolution of cellulose, etc, are closely related to the interaction energy and H-bonds.

As for other chemistries, for example nano science and biotechnology, ILs give people the potential to deal with some unresolved problems and fulfill a task in

green chemical processes. Structural investigations can further provide a deep understanding of the unique properties of ILs and valuable hints for the design of new ILs. Based on this, we believe the following aspects are the most important for future research on ILs. First is to know the quantitative relationship between the structures and the properties of ILs, which will point us in the direction of how we may design efficient ionic liquids for a special application. Another aspect is to study how to scale up the systems with ILs for the chemical engineering processes. Additionally, with the development of materials science and engineering, ILs have found a new stage on which to play a role.

Acknowledgments This work was supported financially by the Projects of International Cooperation and Exchanges NSFC (No. 21210006, 21336002 and 21376242), Beijing Natural Science Foundation (No.2131005) and National High Technology Research and Development Program of China (863 Program) (No. 2012AA063001).

References

1. Walden P (1914) Molecular weights and electrical conductivity of several fused salts. Bull Acad Imp Sci St Petersbourg 8:405–422
2. Li Chum H, Koch VR, Miller LL et al. (1975) Electrochemical scrutiny of organometallic iron complexes and hexamethylbenzene in a room temperature molten salt. J Am Chem Soc 97:3264–3265
3. Fuller J, Carlin RT, Long HCD et al. (1994) Structure of 1-ethyl-3-methylimidazolium hexafluorophosphate: model for room temperature molten salts. J Chem Soc Chem Commun 299–300
4. Wilkes JS, Zaworotko MJ (1992) Air and water stable 1-ethyl-3-methylimidazolium based ionic liquids. J Chem Soc Chem Commun 965–967
5. Hapiot P, Lagrost C (2008) Electrochemical reactivity in room-temperature ionic liquids. Chem Rev 108:2238–2264
6. Nockemann P, Thijs B, Driesen K et al. (2007) Choline saccharinate and choline acesulfamate: ionic liquids with low toxicities. J Phys Chem B 111:5254–5263
7. Pernak J, Syguda A, Mirska I et al. (2007) Choline-derivative-based ionic liquids. Chem Eur J 13:6817–6827
8. Fredlake CP, Crosthwaite JM, Hert DG et al. (2004) Thermophysical properties of imidazolium-based ionic liquids. J Chem Eng Data 49:945–964
9. Raabe G, Köhler J (2008) Thermodynamical and structural properties of imidazolium based ionic liquids from molecular simulation. J Chem Phys 128:154509
10. Weingartner H (2008) Understanding ionic liquids at the molecular level: facts, problems, and controversies. Angew Chem Int Ed 47:654–670
11. Zhang S, Sun N, He X et al. (2006) Physical properties of ionic liquids: database and evaluation. J Phys Chem Ref Data 35:1475–1517
12. Bonhôte P, Dias AP, Papageorgiou N et al. (1996) Hydrophobic, highly conductive ambient-temperature molten salts. Inorg Chem 35:1168–1178
13. Tokuda H, Hayamizu K, Ishii K et al. (2004) Physicochemical properties and structures of room temperature ionic liquids. 1. Variation of anionic species. J Phys Chem B 108:16593–16600
14. Mcewen AB, Ngo HL, Lecompte K et al. (1999) Electrochemical properties of imidazolium salt electrolytes for electrochemical capacitor applications. J Electrochem Soc 146:1687–1697

15. Hyun B, Dzyuba SV, Bartsch RA et al. (2002) Intermolecular dynamics of room-temperature ionic liquids: femtosecond optical Kerr effect measurements on 1-alkyl-3-methylimidazolium bis((trifluoromethyl)sulfonyl)imides. J Phys Chem A 106:7579–7585
16. Every HA, Bishop AG, Macfarlane D et al. (2004) Transport properties in a family of dialkylimidazolium ionic liquids. Phys Chem Chem Phys 6:1758–1765
17. Huddleston JG, Visser AE, Reichert WM et al. (2001) Characterization and comparison of hydrophilic and hydrophobic room temperature ionic liquids incorporating the imidazolium cation. Green Chem 3:156–164
18. Tsuzuki S, Tokuda H, Hayamizu K et al. (2005) Magnitude and directionality of interaction in ion pairs of ionic liquids: relationship with ionic conductivity. J Phys Chem B 109:16474–16481
19. Fitchett BD, Knepp TN, Conboy JC (2004) 1-Alkyl-3-methylimidazolium bis(perfluoroalkylsulfonyl)imide water-immiscible ionic liquids. J Electrochem Soc 151:E219–E225
20. Macfarlane D, Sun J, Golding JJ et al. (2000) High conductivity molten salts based on the imide ion. Electrochim Acta 45:1271–1278
21. Hyk W, Caban K, Donten M et al. (2001) Properties of microlayers of ionic liquids generated at microelectrode surface in undiluted redox liquids. Part II J Phys Chem B 105:6943–6949
22. Earle MJ, Esperanc JMSS, Gilea MA et al. (2006) The distillation and volatility of ionic liquids. Nature 439:831–834
23. Zaitsau DH, Kabo GJ, Strechan AA et al. (2006) Experimental vapor pressures of 1-alkyl-3-methylimidazolium bis(trifluoromethylsulfonyl)imides and a correlation scheme for estimation of vaporization enthalpies of ionic liquids. J Phys Chem A 110:7303–7306
24. Köddermann T, Paschek D, Ludwig R (2008) Ionic liquids: dissecting the heat of vaporization. Chem Phys Chem 9:549–555
25. Blanchard LA, Gu ZY, Brennecke JF (2001) High-pressure phase behavior of ionic liquid/CO_2 systems. J Phys Chem B 105:2437–2444
26. Cammarata L, Kazarian SG, Salterb PA et al. (2001) Molecular states of water in room temperature ionic liquids. Phys Chem Chem Phys 3:5192–5200
27. Devyatykh GG, Sennikov PG (1995) Spectroscopic determination and study of the molecular state of water in ultrapure volatile inorganic substances. Russ Chem Rev 64:817–830
28. Rivera-Rubero S, Baldelli S (2004) Influence of water on the surface of hydrophilic and hydrophobic room-temperature ionic liquids. J Am Chem Soc 126:11788–11789
29. Bhargava BL, Balasubramanian S (2006) Layering at an ionic liquid–vapor interface: a molecular dynamics simulation study of [bmim][PF_6]. J Am Chem Soc 128:10073–10078
30. Rogers RD (2007) Reflections on ionic liquids. Nature 447:917–918
31. Katritzky AR, Lomaka A, Petrukhin R et al. (2002) Correlation of the melting point for pyridinium bromides, potential ionic liquids. J Chem Inf Comput Sci 42:71–74
32. Elaiwi A, Hitchcock PB, Seddon KR et al. (1995) Hydrogen bonding in imidazolium salts and its implications for ambient-temperature halogenoaluminate(llI) ionic liquids. J Chem Soc Dalton Trans 3467–3472
33. Dymek CJ, Grossie DA, Fratini AV et al. (1989) Evidence for the presence of hydrogen-bonded ion-ion interactions in the molten salt precursor, 1-methyl-3-ethylimidazolium chloride. J Mol Struct 213:25–34
34. Turner EA, Pye CC, Singer RD (2003) Use of ab initio calculations toward the rational design of room temperature ionic liquids. J Phys Chem A 107:2277–2288
35. Reichert WM, Holbrey JD, Swatloski RP et al. (2007) Solid-state analysis of low-melting 1,3-dialkylimidazolium hexafluorophosphate salts (ionic liquids) by combined X-ray crystallographic and computational analyses. Cryst Growth Des 7:1106–1114
36. Matsumoto K, Hagiwara R (2007) Structural characteristics of alkylimidazolium-based salts containing fluoroanions. J Fluorine Chem 128:317–331
37. Xue H, Verma R, Shreeve JM (2006) Review of ionic liquids with fluorine-containing anions. J Flour Chem 127:159–176

38. Swatloski RP, Holbrey JD, Rogers RD (2003) Ionic liquids are not always green: hydrolysis of 1-butyl-3-methylimidazolium hexafluorophosphate. Green Chem 5:361–363
39. Choudhury AR, Winterton N, Steiner A et al. (2005) In situ crystallization of low-melting ionic liquids. J Am Chem Soc 127:16792–16793
40. Hasan M, Kozhevnikov IV, Siddiqui MRH et al. (2001) N, N-Dialkylimidazolium chloroplatinate(II), chloroplatinate(IV), and chloroiridate(IV) salts and an N-heterocyclic carbene complex of platinum(II): synthesis in ionic liquids and crystal structures. Inorg Chem 40:795–800
41. Matsumoto K, Hagiwara R, Yoshida R et al. (2004) Syntheses, structures and properties of 1-ethyl-3-methylimidazolium salts of fluorocomplex anions. Dalton Trans 144–149
42. Matsumoto K, Hagiwara R, Mazej Z et al. (2006) Crystal structures of frozen room temperature ionic liquids,1-ethyl-3-methylimidazolium tetrafluoroborate ($EMImBF_4$), hexafluoroniobate ($EMImNbF_6$) and hexafluorotantalate ($EMImTaF_6$), determined by low-temperature X-ray diffraction. Solid State Sci 8:1250–1257
43. Luo H, Baker GA, Dai S (2008) Isothermogravimetric determination of the enthalpies of vaporization of 1-alkyl-3-methylimidazolium ionic liquids. J Phys Chem B 112:10077–10081
44. Armstrong JP, Hurst C, Jones RG et al. (2007) Vapourisation of ionic liquids. Phys Chem Chem Phys 9:982–990
45. Hunt PA, Kirchner B, Welton T (2006) Characterising the electronic structure of ionic liquids: an examination of the 1-butyl-3-methylimidazolium chloride ion pair. Chem Eur J 12:6762–6775
46. Dong K, Song Y, Liu X et al. (2012) Understanding structures and hydrogen bonds of ionic liquids at the electronic level. J Phys Chem B 116:1007–1017
47. Dong K, Zhang S, Wang D et al. (2006) Hydrogen bonds in imidazolium ionic liquids. J Phys Chem A 110:9775–9782
48. Fumino K, Wulf A, Ludwig R (2009) Hydrogen bonding in protic ionic liquids: reminiscent of water. Angew Chem Int Ed 48:3184–3186
49. Zhao W, Leroy FD, Heggen B et al. (2009) Are there stable ion-pairs in room-temperature ionic liquids? Molecular dynamics simulations of 1-n-butyl-3-methylimidazolium hexafluorophosphate. J Am Chem Soc 131:15825–15833
50. Liu Z, Huang S, Wang W (2004) A refined force field for molecular simulation of imidazolium-based ionic liquids. J Phys Chem B 108:12978–12989
51. Talaty ER, Raja S, Storhaug VJ et al. (2004) Raman and infrared spectra and ab initio calculations of $C_{2\text{-}4}$MIM imidazolium hexafluorophosphate ionic liquids. J Phys Chem B 108:13177–13184
52. Wang Y, Voth GA (2005) Unique spatial heterogeneity in ionic liquids. J Am Chem Soc 127:12192–12193
53. Izvekov S, Violi A, Voth GA (2005) Systematic coarse-graining of nanoparticle interactions in molecular dynamics simulation. J Phys Chem B Lett 109:17019–17024
54. Liu X, Zhou G, Zhang S (2008) Molecular dynamics simulation of acyclic guanidinium-based ionic liquids. Fluid Phase Equilibr 272:1–7
55. Mizuse K, Mikami N, Fujii A (2010) Infrared spectra and hydrogen-bonded network structures of large protonated water clusters H + (H2O)n (n = 20-200). Angew Chem Int Ed 49:10119–10122
56. Russina O, Triolo A, Gontrani L, Caminiti R (2012) Mesoscopic structural heterogeneities in room-temperature ionic liquids. J Phys Chem Lett 3:27–33
57. Hardacre C, McMath SEJ, Nieuwenhuyzen M, Bowron DT, Soper AK (2003) Liquid structure of 1,3-dimethylimidazolium salts. J Phys Condens Matter 15:S159–S166
58. Canongia Lopes JN, Padua AAH (2006) Nanostructural organization in ionic liquids. J Phys Chem B110:3330–3335
59. Triolo A, Russina O, Bleif H-J, Di Cola E (2007) Nanoscale segregation in room temperature ionic liquids. J Phys Chem B111:4641–4644

60. Auon B, Goldbatch A, Gonzalez M, Kohara S, Rice DL, Saboungi M-L (2011) Nanoscale heterogeneity in alkyl-methylimidazolium bromide ionic liquids. J Chem Phys 134:104509
61. Zahn S, Uhlig F, Thar J et al. (2008) Intermolecuar forces in an ionic liquid ([Mmim]Cl) versus those in a typical salt (NaCl). Angew Chem Int Ed 47:3639–3641
62. Crowhurst L, Mawdsley PR, Perez-Arlandis JM et al. (2003) Solvent-solute interactions in ionic liquids. Phys Chem Chem Phys 5:2790–2794
63. Hunt PA, Gould IR (2006) Structural characterization of the 1-butyl-3-methylimidazolium chloride ion pair using ab initio methods. J Phys Chem A 110:2269–2282
64. Abdul-Sada AK, Greenway AM, Hitchcock PB et al. (1986) Upon the structure of room temperature halogenoaluminate ionic liquids. J Chem Soc Chem Commun 1753–1754
65. Khupse ND, Kumar A (2010) Contrasting thermosolvatochromic trends in pyridinium-, pyrrolidinium-, and phosphonium-based ionic liquids. J Phys Chem B 114:376–381
66. Tokuda H, Tsuzuki S, Susan MBH et al. (2006) How ionic are room-temperature ionic liquids? An indicator of the physicochemical properties. J Phys Chem B 110:19593–19600
67. Fukaya Y, Sugimoto A, Ohno H (2006) Superior solubility of polysaccharides in low viscosity, polar, and halogen-free 1,3-dialkylimidazolium formates. Biomacromolecules 7:3295–3297
68. Dieter KM, Dymek CJJ, Heimer NE et al. (1988) Ionic structure and interactions in 1-methyl-3-ethylimidazolium chloride-aluminum chloride molten salts. J Am Chem Soc 110:2722–2726
69. Remsing RC, Wildin JL, Rapp AL et al. (2007) Hydrogen bonds in ionic liquids revisited: $^{35/37}$Cl NMR studies of deuterium isotope effects in 1-n-butyl-3-methylimidazolium chloride. J Phys Chem B 111:11619–11621
70. Hardacre C, Holbrey JD, Mcmath SEJ et al. (2003) Structure of molten 1,3-dimethylimidazolium chloride using neutron diffraction. J Chem Phys 118:273–279
71. Heimer NE, Sesto RED, Meng Z et al. (2006) Vibrational spectra of imidazolium tetrafluoroborate ionic liquids. J Mol Liq 124:84–95
72. Holbrey JD, Reichert WM, Nieuwenhuyzen M et al. (2003) Liquid clathrate formation in ionic liquid–aromatic mixtures. Chem Commun 476–477
73. Hardacre C, Mcmath SEJ, Nieuwenhuyzen M et al. (2003) Liquid structure of 1, 3-dimethylimidazolium salts. J Phys Condens Matter 15:S159–S166
74. Rijnberg E, Richter B, Thiele KH et al. (1998) A homologous series of homoleptic zinc bis (1,4-di-tert-butyl-1,4-diaza-1,3-butadiene) complexes: Kx[Zn(t-BuNCHCHN-t-Bu)2], Zn (t-BuNCHCHN-t-Bu)2, and [Zn(t-BuNCHCHN-t-Bu)2](OTf)x (x = 1, 2). Inorg Chem 37:56–63
75. Umebayashi Y, Fujimori T, Sukizaki T et al. (2005) Evidence of conformational equilibrium of 1-ethyl-3-methylimidazolium in its ionic liquid salts: Raman spectroscopic study and quantum chemical calculations. J Phys Chem A 109:8976–8982
76. Roth C, Peppel T, Fumino K et al. (2010) The importance of hydrogen bonds for the structure of ionic liquids: single-crystal X-ray diffraction and transmission and attenuated total reflection spectroscopy in the terahertz region. Angew Chem Int Ed 49:10221–10224
77. Fumino K, Wulf A, Ludwig R (2008) Strong, localized, and directional hydrogen bonds fluidize ionic liquids. Angew Chem Int Ed 47:8731–8734
78. Gjikaj M, Leye J-C, Xie T et al. (2010) Structural and spectroscopic elucidation of imidazolium and pyridinium based hexachloridophosphates and niobates. CrystEngComm 12:1474–1480
79. Deetlefs M, Hardacre C, Nieuwenhuyzen M et al. (2006) Liquid structure of the ionic liquid 1,3-dimethylimidazolium bis{(trifluoromethyl)sulfonyl}amide. J Phys Chem B 110: 12055–12061
80. Holbrey JD, Reichert WM, Rogers RD (2004) Crystal structures of imidazolium bis(trifluoromethanesulfonyl)-imide 'ionic liquid' salts: the first organic salt with a cis-TFSI anion conformation. Dalton Trans 2267–2271

81. Wulf A, Fumino K, Ludwig R (2010) Spectroscopic evidence for an enhanced anion–cation interaction from hydrogen bonding in pure imidazolium ionic liquids. Angew Chem Int Ed 49:449–453
82. Shetty PH, Youngberg PJ, Kersten BR et al. (1987) Solvent properties of liquid organic salts used as mobile phases in microcolumn reversed-phase liquid chromatography. J Chromatogr 411:61–79
83. Ding J, Welton T, Armstrong DW (2004) Chiral ionic liquids as stationary phases in gas chromatography. Anal Chem 76:6819–6822
84. Geissler PL, Dellago C, Chandler D et al. (2001) Autoionization in liquid water. Science 291:2121–2124
85. Dong K, Zhang S (2012) Hydrogen bonds: a structural insight into ionic liquids. Chem Eur J 18:2748–2761
86. Downard A, Earle MJ, Hardacre C et al. (2004) Structural studies of crystalline 1-alkyl-3-methylimidazolium chloride salts. Chem Mater 16:43–48
87. Berg RW, Deetlefs M, Seddon KR et al. (2005) Raman and ab initio studies of simple and binary 1-alkyl-3-methylimidazolium ionic liquids. J Phys Chem B 109:19018–19025
88. Wang Y, Voth GA (2006) Tail aggregation and domain diffusion in ionic liquids. J Phys Chem B 110:18601–18608
89. Canongia Lopes JN, Padua AH (2006) Nanostructural organization in ionic liquids. J Phys Chem B 110:3330–3335
90. Xiao D, Rajian JR, Cady A et al. (2007) Nanostructural organization and anion effects on the temperature dependence of the optical Kerr effect spectra of ionic liquids. J Phys Chem B 111:4669–4677
91. Soutullo MD, Odom CI, Wicker BF et al. (2007) Reversible CO_2 capture by unexpected plastic-, resin-, and gel-like ionic soft materials discovered during the combi-click generation of a TSIL library. Chem Mater 19:3581–3583
92. Huddleston JG, Willauer HD, Swatloski RP et al. (1998) Room temperature ionic liquids as novel media for 'clean' liquid–liquid extraction. Chem Commun 1765–1766
93. Holbrey JD, Lopez-Martin I, Rothenberg G et al. (2008) Desulfurisation of oils using ionic liquids: selection of cationic and anionic components to enhance extraction efficiency. Green Chem 10:87–92
94. Xie LL, Favre-Reguillon A, Wang XX et al. (2008) Selective extraction of neutral nitrogen compounds found in diesel feed by 1-butyl-3-methyl-imidazolium chloride. Green Chem 10:524–531
95. Domanska U, Pobudkowska A, Krolikowski M (2007) Separation of aromatic hydrocarbons from alkanes using ammonium ionic liquid C_2NTf_2 at $T = 298.15$ K. Fluid Phase Equilibr 259:173–179
96. Zhang SG, Zhang QL, Zhang ZC (2004) Extractive desulfurization and denitrogenation of fuels using ionic liquids. Ind Eng Chem Res 43:614–622
97. Cao Y, Xing H, Yang Q et al. (2012) Separation of soybean isoflavone aglycone homologues by ionic liquid-based extraction. J Agric Food Chem 60:3432–3440
98. Dong K, Cao Y, Yang Q et al. (2012) Role of hydrogen bonds in ionic-liquid-mediated extraction of natural bioactive homologues. Ind Eng Chem Res 51:5299–5308
99. Anderson JL, Ding J, Welton T et al. (2002) Characterizing ionic liquids on the basis of multiple solvation interactions. J Am Chem Soc 124:14247–14254
100. Pinkert A, Marsh KN, Pang S et al. (2009) Ionic liquids and their interaction with cellulose. Chem Rev 109:6712–6728
101. Rinaldi R, Palkovits R, Schüth F (2008) Depolymerization of cellulose using solid catalysts in ionic liquids. Angew Chem Int Ed 47:8047–8050
102. Vispute TP, Zhang H, Sanna A et al. (2010) Renewable chemical commodity feedstocks from integrated catalytic processing of pyrolysis oils. Science 330:1222–1227
103. Swatloski RP, Spear SK, Holbrey JD et al. (2002) Dissolution of cellose with ionic liquids. J Am Chem Soc 124:4974–4975

104. Tan SSY, Macfarlane DR, Upfal J et al. (2009) Extraction of lignin from lignocellulose at atmospheric pressure using alkylbenzenesulfonate ionic liquid. Green Chem 11:339–345
105. Qin Y, Lu X, Sun N et al. (2010) Dissolution or extraction of crustacean shells using ionic liquids to obtain high molecular weight purified chitin and direct production of chitin films and fibers. Green Chem 12:968–971
106. Xie H, Li S, Zhang S (2005) Ionic liquids as novel solvents for the dissolution and blending of wool keratin fibers. Green Chem 7:606–608
107. Remsing RC, Swatloski RP, Rogers RD et al. (2006) Mechanism of cellulose dissolution in the ionic liquid 1-n-butyl-3-methylimidazolium chloride: a ^{13}C and $^{35/37}Cl$ NMR relaxation study on model systems. Chem Commun 28:1271–1273
108. Sun N, Rahman M, Qin Y et al. (2009) Complete dissolution and partial delignification of wood in the ionic liquid 1-ethyl-3-methylimidazolium acetate. Green Chem 11:646–655
109. Liu H, Sale KL, Holmes BM et al. (2010) Understanding the interactions of cellulose with ionic liquids: a molecular dynamics study. J Phys Chem B 114:4293–4301
110. Garcia H, Ferreira R, Petkovic M et al. (2010) Dissolution of cork biopolymers in biocompatible ionic liquids. Green Chem 12:367–369
111. Jaeger DA, Tucker CE (1989) Diels-Alder reactions in ethylammonium nitrate, a low-melting fused salt. Tetrahedron Lett 30:1785–1788
112. Aggarwal A, Lancaster NL, Sethi AR et al. (2002) The role of hydrogen bonding in controlling the selectivity of Diels–Alder reactions in room-temperature ionic liquids. Green Chem 4:517–520
113. Anthony JL, Maginn EJ, Brennecke JF (2002) Solubilities and thermodynamic properties of gases in the ionic liquid 1-n-butyl-3-methylimidazolium hexafluorophosphate. J Phys Chem B 106:7315–7320
114. Yuan X, Zhang S, Liu J et al. (2007) Solubilities of CO_2 in hydroxyl ammonium ionic liquids at elevated pressures. Fluid Phase Equilibr 257:195–200
115. Zhang S, Chen Y, Ren RX-F et al. (2005) Solubility of CO_2 in sulfonate ionic liquids at high pressure. J Chem Eng Data 50:230–233
116. Blanchard LA, Hancu D, Beckman EJ et al. (1999) Green processing using ionic liquids and CO_2. Nature 399:28–29
117. Huanga J, Riisager A, Wasserscheidb P et al. (2006) Reversible physical absorption of SO_2 by ionic liquids. Chem Commun 38:4027–4029
118. Huang X, Margulis CJ, Li Y et al. (2005) Why is the partial molar volume of CO_2 so small when dissolved in a room temperature ionic liquid? Structure and dynamics of CO_2 dissolved in $[Bmim]^+ [PF_6]^-$. J Am Chem Soc 127:17842–17851
119. Scovazzo P, Camper D, Kieft J et al. (2004) Regular solution theory and CO_2 gas solubility in room-temperature ionic liquids. Ind Eng Chem Res 43:6855–6860
120. Kerlé D, Ludwig R, Geiger A et al. (2009) Temperature dependence of the solubility of carbon dioxide in imidazolium-based ionic liquids. J Phys Chem B 113:12727–12735
121. Paschek D, Köddermann T, Ludwig R (2008) The solvophobic solvation and interaction of small apolar particales in imidazolium-based ionic liquids. Phys Rev Lett 100:115901–115904